Magnetic effects in dense holographic nuclear matter and Neutron Stars

Master Thesis

Nikolaos Karastathis

Student Number : 6215602

Graduate School of Natural Sciences

Institute for Theoretical Physics

January 2020

Supervisors :

Assoc. Prof. U. Gürsoy

Dr. M. Järvinen

Success is not final,
failure is not fatal:
it is the courage to continue that
counts.

WINSTON S. CHURCHILL

Abstract

Neutron stars consist of QCD matter at extreme densities, which is a regime in which first principle QCD calculations cannot be performed. Also, neutron stars often have extremely large magnetic fields. Therefore, in this work, we investigate a different approach to strong coupling theories: we employ the gauge/gravity duality and we study how it can be used in QCD. Hence, we consider a holographic model for QCD, named V-QCD, and use this to compute the phase diagram, the equation of state and more thermodynamic quantities at finite density and magnetic field. Lastly, the equation of state is used to investigate the consequences for neutron stars. We see that our holographic model produces potentially realistic results for the core region.

Contents

1 Introduction

During the 50's multiple experiments with particles took place that shed light to a variety and ever growing number of new particles, the hadrons. Researchers realized that all this amount of hadrons was a hint that this the particle zoo cannot be the final answer and there should exist some fundamental particles aside from the ones they already knew. They would be able to play the role of the buildings blocks of the increasing number of newly discovered particles.

Motivated by the above, the formulation of Quantum Chromodynamics (QCD) came to existence. QCD describes the strong force which is dominant in the substituents of atomic nuclei, namely quarks and gluons. Quarks are bound inside protons and neutrons under normal circumstances and gluons are the force carriers. Particles described by QCD are characterized by two parameters, colour (hence "chromo" in QCD) and flavour. QCD is a strongly coupled theory that has three key features which are going to be discussed in detail later. These are confinement, chiral symmetry breaking and asymptotic freedom. Both theorists and experimentalists are trying to tackle the peculiarities of QCD. The most difficult part is precisely the fact that since it is strongly coupled, perturbation theory fails in low energies. Hence, people had to come up with other techniques to describe its key features. Lattice QCD is one of these techniques that is successful but only to zero values of chemical potential. In 1997 though, Maldacena [4] in his groundbreaking work in which he modeled strongly coupled theories through higher dimensional gravity, opened a new door to approach not only QCD, but strongly coupled theories in general.

Since then, there has been a significant effort to reproduce a holographic model that corresponds to the salient features of QCD [24], [25]. The advantage of studying the problem this way is that once a holographic model has been established and gives reasonable results, then we can gain insight on more QCD phenomena like quark-gluon plasma for example, and also discover completely new aspects of our theory.

In this thesis, we work on a holographic model that seems to describe successfully QCD at the region where neutron stars in the QCD phase diagram reside, and we examine how baryons are affected when a constant external magnetic field is applied. We will use the resulting Equation of State to solve the Tolman-Oppenheimer-Volkoff (TOV) equation for neutron stars and see if a reasonable Mass/Radius curve comes out.

In Chapter 2 a brief overview of QCD and the techniques that we have so far will be discussed. In Chapter 3 AdS/CFT is going to be introduced and the connection with QCD is going to be made. In Chapter 4, the most recent holographic models resulting to the model we are working with in this thesis, namely V-QCD, are going to be described. The magnetic field and neutron stars are going to be introduced and more of our work is continued in Chapter 5, including an ansatz to approximate baryons. Finally, in Chapter 6 Grand potential, neutron stars and further results are going to be given and discussed.

2 Elements of Quantum Chromodynamics

2.1 Brief overview of QCD

There are four known fundamental forces in the universe. Gravity, Electromagnetic force, the Weak and the Strong interaction. The last three are described successfully within the Standard model of Particle Physics. QCD is part of the Standard Model and describes the Strong interaction which is responsible for the strong nuclear force. This force is what binds quarks together in order for them to form mesons and baryons. The force carriers are the gauge fields in the field theoretic description of the theory and are called gluons. Quarks come in six flavours, namely up, down, top, bottom, charm, strange and each flavour comes in three colours. The masses of up and down are not known precisely because they have not been detected as isolated particles. It is worth mentioning at this point that quarks can actually change their flavour due to weak interactions and that also gluons do not carry flavour, but only colour. QCD is described by an SU(3) gauge theory of the Yang-Mills type [1] and the Lagrangian reads :

$$\mathcal{L} = -\frac{1}{4} F^{\alpha}_{\mu\nu} F^{\mu\nu}_{\alpha} + \bar{\Psi}_{\nu}(i\gamma^{\mu} D_{\mu} - m)\Psi^{\nu} \tag{1}$$

where the field strength tensor $F^{\alpha}_{\mu\nu}$ is defined as follows :

$$F^{\alpha}_{\mu\nu} = \partial_{\mu} A^{\alpha}_{\nu} - \partial_{\nu} A^{\alpha}_{\mu} + g f^{abc} A^{b}_{\mu} A^{c}_{\nu} \tag{2}$$

the covariant derivative has the form :

$$D_{\mu} = \partial_{\mu} - igA^{\alpha}_{\mu} t^{\alpha} \tag{3}$$

and the commutation relations of SU(3) are given by the following relation :

$$[t_b, t_c] = i f^{a}_{bc} t_a \tag{4}$$

A^{α}_{μ} is the gauge field (gluons) in the adjoint representation, Ψ are the fermion fields (quarks) in the fundamental representation, f^{abc} are the structure constants of the SU(3) group and t^{α} are its generators.

There are **three key features** of this theory that are relevant for our work :

- **Chiral Symmetry Breaking**

  The QCD Lagrangian helps us understand the symmetries of our theory. It enjoys what is

called chiral symmetry [2]. The chiral symmetry is eminent by considering two flavours, up and down because their masses are very light and approximately the same. We consider the limit of massless quarks. The fermion field now has the form $\Psi = \begin{pmatrix} u \\ d \end{pmatrix}$ and $m = \begin{pmatrix} m_u & 0 \\ 0 & m_d \end{pmatrix}$ where m_u and m_d are the masses of the up and down quarks. Now our Lagrangian is divided to left (L) and right (R) fields. In the limit of zero quark mass the full chiral symmetry of can now be expressed in the following manner :

$$SU(2)_V \times SU(2)_A \times U(1)_V \times U(1)_A \tag{5}$$

The invariance under $U(1)_V$ is related to the conservation of baryon number, while the invariance under $SU(2)_V$ corresponds to Heisenberg's isospin symmetry. However, the vacuum breaks the axial symmetries as it is not invariant under transformations of the form $SU(2)_A \times U(1)_A$. The breaking of this symmetry produces a quark-antiquark condensate $\langle q\bar{q} \rangle \neq 0$ which acts as an order parameter and is telling us that the vacuum of space is populated by quark-antiquark pairs at no energy cost. This is analogous to what happens in a superconductor, where pairs of electron form a condensate. The resulting ground state has an indefinite number of quark-anti-quark pairs that fills the vacuum while still preserving Lorentz invariance. For this to happen, we must be working on the strongly coupled regime and the quark pairs must have opposite quantum numbers for both momentum and angular momentum. It is worth mentioning that $U(1)_A$ is also broken by the chiral anomaly.

In reality though, quarks masses do not vanish which is why the Chiral symmetry in this context is characterized as approximate. In this sense, since $\langle q\bar{q} \rangle \neq 0$ breaks axial SU(2) symmetry, pions can be regarded as approximate light Goldstone bosons, and hence, the fact that the pion mass is substantially smaller than the mass of other hadrons is explained.

- **Colour confinement** QCD has the property that physical states correspond to colour singlets $(q^\dagger q)$ transforming under SU(3). In more detail,

$$\begin{aligned} & q^a \to U_{ab} q^b \\ & (q^\dagger)^a \to (q^\dagger)^b U_{ba} \\ & \text{where} \quad U \in SU(3) \quad \text{and} \quad U^+ U = 1 \end{aligned} \tag{6}$$

This fact is what we call "colour confinement" [2]. We can imagine it like the figure shown above (1). A quark-antiquark pair is being held together by an invisible string which is

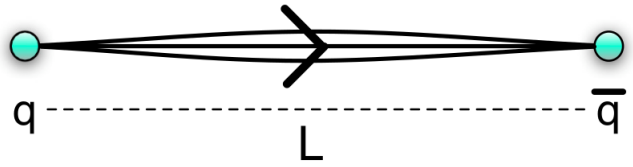

Figure 1: Taken from [31]. The colour confinement is depicted in the picture. Between a quark anti-quark pair a string of length L can be realized to hold them together.

realised as the strong force. As we try to tear the pair apart the force increases indefinitely in a linear fashion via the following potential [31] :

$$V_{q\bar{q}}(L) = \sigma_0 L + ... \tag{7}$$

where L is the separation between the quark and the antiquark and σ_0 is the string tension. This phenomenon of "infrared slavery" although we have strong indications of its existence is non-perturbative by nature, hence perturbation theory fails and we need a different theoretical mechanism to describe it.

It is believed that the this confining mechanism can break down and lead our theory to a deconfined phase under extreme conditions like high temperatures (e.g. extremely energetic heavy-ion collisions) or very high densities (e.g. in neutron stars). It is speculated that the deconfined phase was present in the early stages of the universe. Nowadays, experiments with heavy-ions collisions are being made to study QCD in the quark-gluon plasma state, where quarks and gluons are no longer confined.

- **Asymptotic freedom** QCD is a non-Abelian gauge theory. In general, these theories exhibit the property of asymptotic freedom which means that the running gauge field coupling tends to vanish logarithmically at small distances [5], [2]. In other words, as the energy scale increases the value of the coupling constant becomes smaller meaning that the interactions are weaker at this scale. This can also be seen by the beta function for a general $SU(N_c)$ theory with N_f flavours:

$$\beta(g) = \frac{dg(\mu)}{d\log(\mu)} = -\frac{g^2}{16\pi^2}(\frac{11N_c}{3} - \frac{2N_f}{3}) \tag{8}$$

The beta function vanishes at zero coupling. In first order as can be seen above it is negative for $\frac{N_f}{N_c} < \frac{11}{2}$. This is in accordance with the asymptotic freedom statement and also gives

us the advantage to use perturbation theory at small gauge couplings. These theoretical claims have been confirmed by experiment.

2.2 Lattice QCD

Phenomena involving large momentum transfer imply the small value of the coupling constant, where perturbation theory in QCD is reliable. In this chapter we are going to introduce a different approach which allows us to study phenomena where the coupling constant is of order of unity and perturbative QCD fails. Lattice QCD is such a tool introduced by Wilson in 1974 [9] which provides a way to calculate things like the hadronic spectrum, the matrix elements of the corresponding operators of these hadronic states, but also study confinement, chiral symmetry breaking and the role of topology in the system. Lattice QCD, being an intrinsically Euclidean formulation is not well-suited for calculating certain important dynamical observables such as transport coefficients or any sort of real-time correlation functions in the quark-gluon plasma for instance.

Lattice approach

The basic idea is to approach QCD on a four-dimensional Euclidean space of discrete space-time points rather than in the continuum [5]. Quarks and gluons can only exist on lattice points and travel over connection lines. In principle, it is a non-perturbative implementation of field theory using the Feynman path integral technique. The distance α between these points acts as a cut-off for both small and large momenta singularities that occur in the field theory.
We have to work in Euclidean space-time so as the volume and the temperature of the theory is associated to the number of points. The partition function reads :

$$Z = \int \mathcal{D}A_\mu \mathcal{D}\Psi \mathcal{D}\bar{\Psi} e^{-S} \tag{9}$$

where S is the following action :

$$\mathcal{S} = \int d^4x (\frac{1}{4} F_{\mu\nu} F^{\mu\nu} - \bar{\Psi} \not{\mathcal{D}} \Psi) \tag{10}$$

$F_{\mu\nu}$ is defined in (2) and $\not{\mathcal{D}}$ is the Dirac operator. Fermions (quarks) are represented by Grassmann anti-commuting numbers Ψ and $\bar{\Psi}$ and when integrated out the partition function can be rewritten as :

$$Z = \int \mathcal{D}A_\mu \det \not{\mathcal{D}} e^{\int d^4x (-\frac{1}{4} F_{\mu\nu} F^{\mu\nu})} \tag{11}$$

Bosons (gluons) are represented by the commuting gauge fields A_μ. It is obvious in this context that the fermionic contribution is contained in the $\det \not{\mathcal{D}}$ term leaving the partition function

an integral only over the background gauge fields. Hence, the action can be rewritten : $S = S_{gauge} + S_{fermions} = \int d^4x(-\frac{1}{4}F_{\mu\nu}F^{\mu\nu}) - (\det \not{D})$. In this point it is worth mentioning that the "quenched" approximation of QCD refers that the above determinant is taken to be constant which implies that the vacuum polarization effects are removed and it is used in simulations. Further technicalities on the theoretical approach of lattice QCD are explained in detail in [5].

Estimates of Lattice QCD

In our work we are interested in studying the thermodynamics of QCD. Hence, it is logical to refresh our memory on the thermodynamic quantities that are relevant. Keep in mind that QCD as introduced earlier is an SU(3) theory which belongs in the more general family of SU(N) theories whose thermodynamics quantities are going to be given. Starting from the partition function $\mathcal{Z}(T,V)$ the free energy density is :

$$f = -\frac{T}{V}\ln \mathcal{Z}(T,V) \tag{12}$$

the energy density and pressure :

$$\epsilon = \frac{T^2}{V}\frac{\partial \ln \mathcal{Z}(T,V)}{\partial T} \tag{13}$$

$$p = T\frac{\partial \ln \mathcal{Z}(T,V)}{\partial V} \tag{14}$$

but when considering large homogeneous systems this holds : $p = -f$. So the quantities above can be re expressed as :

$$\frac{\epsilon + p}{T} = \frac{\partial p}{\partial T} \tag{15}$$

$$\text{and} \quad \epsilon - 3p = T^5\frac{\partial}{\partial T}(\frac{p}{T^4}) \tag{16}$$

whereas the entropy density is :

$$s = \frac{\epsilon + p}{T} \tag{17}$$

Temperature and the volume are dependent by the lattice size $N_\sigma^3 \times N_\tau$ and the lattice spacing α with the following relations :

$$T^{-1} = N_\tau \alpha, \quad V = (N_\sigma \alpha)^3 \tag{18}$$

The difficulty when trying to tackle this problem is the direct calculation of the partition function. People have turned into Monte Carlo simulations but in [39] the expectation value of the action is studied. This is connected to the confined or deconfined phase transitions of the theory where

the proper observables are the string tension or the critical temperature. The order of the aforementioned phase transitions is expressed through the study of the susceptibilities which clearly shows that the number of flavours N_f play an important role although the number of the colours N_c are not so relevant giving us the freedom to take this number to infinity to construct new models as will be shown later on.

Lattice QCD gives promising results in accordance with experiments [30] using numerical simulations hinting theoretical physicists to use this theory as a boundary check on the models they come up with. Although, Lattice QCD imposes also an infamous problem on its own apart from the failure of an analytic solution to the partition function. This problem is often called the "sign problem" [27]. So far all the modelling is being done at zero chemical potential μ. When one tries to add a value to the chemical potential, then the Dirac operator has also a $\bar{\Psi}\mu\gamma^0\Psi$ component. Since the Dirac operator is calculated through a determinant, this means that a phase factor is now present who serves as a weight leading to complex eigenvalues which can also be negative.This leads to two possibilities, the first being an imaginary chemical potential and the second being the existence of two degenerate quarks, e.g. $m_u = m_d$ and $\mu_u = -\mu_d$. Monte Carlo simulations are not doable at a non-zero chemical potential although work to overcome these issues is being done towards that direction. An example is [27]. Other approaches that are worth mentioning are effective field theory and perturbative methods but we will not elaborate more on those since we will not use them.

2.3 QCD phase diagram

At this point, having mentioned a few important facts about QCD it is fruitful to introduce and discuss a specific QCD phase diagram [13], [26]. The one we are working with is a diagram of temperature T (in the vertical axis) and the chemical potential μ_B (in the horizontal axis) which is produced from a combination of theoretical research and experiments (RHIC, LHC, FAIR SIS 300). It describes the state of the matter in different values of T and μ_B that can be either found in the universe or are highly speculated from our current understanding of the theory. For this reason the diagram is not characterized by absolute certainty as a lot of its regions are being explored experimentally. Nevertheless, it serves us as a very good tool. When constructing a new model for our theory using holography for example, which is the topic of this thesis, we can check if our model agrees on the areas that are proven experimentally to behave as the diagram suggests giving us a green light to push our model further.

Before jumping into the diagram itself let us briefly recall the classification of phase transitions. The characteristic of a 1st order phase transition is that the first derivative of the free energy is discontinuous at T_c. This means that at a critical temperature T_c, part of the system is in one phase and the rest is in another phase. On a 2nd order phase transition though, both the free energy and its first derivative are continuous, unlike the second derivative at T_c. The third kind of phase transition is the analytical crossover. In this case the free energy and all its derivatives are continuous at the critical temperature. This means that the change will be smooth without discontinuities making it more difficult to identify which phase you are in the diagram.

An impression that we have on the QCD phase diagram is shown in figure 2. Starting from the left part of the diagram, in the slice for μ_B equal to zero up to arbitrary values of temperature, lattice simulations are applicable. The phase described by large values of temperature on that slice, is believed to have existed during the early stages of the universe and by cooling down, hadrons were formed. Chiral Symmetry is broken in the hadronic phase in general up to a certain critical temperature and is restored elsewhere. Quarks and gluons here are confined forming up the hadrons, but as we move up to higher temperatures there is a crossover leading to the deconfined phase. In this area quarks and gluons are no longer confined and are the only form of matter we encounter. This form of matter is called Quark-Gluon plasma (QGP). Chiral symmetry is also restored at this point. One would expect QGP to behave as an ideal gas. Surprisingly, its behaviour is closer to a perfect fluid with a very small shear viscosity. The form

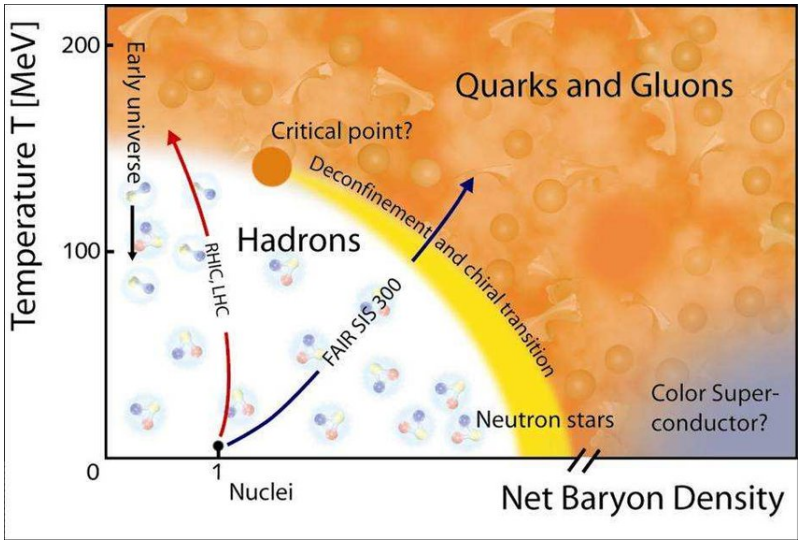

Figure 2: Taken from [6]. Impression of QCD phase diagram. It depicts the 3 phases of QCD matter with respect to temperature and net baryon density.

of matter as we know it, appears when QGP cools down. Protons and neutrons are formed and when cooled even further are able to form nuclear matter. Experiments are being held at RHIC and LHC where for increasing temperature one starts from the hadronic phase and attempts to investigate the plasma phase.

Moving to higher temperatures and larger μ, due to chiral symmetry restoration, the area of the phase transition where the hadron gas becomes QGP is not strict, as it is obvious from the diagram. In this area the most effective theoretical tool we posses is perturbation theory. This happens because at high energies the coupling is weak making perturbations possible. As we continue further at high densities and low temperatures ($T < 100MeV$), there lies a colour superconducting phase in which up and down quarks with two out of three colors pair and form a condensate in analogy to BCS theory. It is speculated that the transition from the colour superconductor to the QGP is of 1st order. In the middle of the diagram where the temperature is low and the baryonic density is increased (cold dense QCD matter) much effort is being done to find a suitable theoretical model as this area is mainly uninvestigated making our knowledge limited. In this area though, as is obvious from the diagram is where neutron stars can be found. The reason that there is not much solid knowledge in this area is because for the slice $\mu_B = 0$ up to high temperatures we can use lattice simulations, for high energies we can use perturbations

but in this particular area lattice simulations fail due to the sign problem and perturbation theory also fails because the coupling is strong. Hence, in order for us to study cold and dense QCD matter and apply our results to neutron stars we have to use a different technique. This technique is the AdS/CFT correspondence and is going to be introduced in the next section.

3 Gauge/Gravity duality

In this section we are going to review some basic concepts of the duality. The general idea of AdS/CFT correspondence lies in the boundary of AdS. Locally the boundary appears to be flat, so making use of the Minkowski spacetime to describe it, makes sense. This particular spacetime is also used in field theory calculations hinting us to look further into AdS. Therefore, in the boundary one can make non-gravitational calculations using conformal field theory, whereas in the bulk one is free to use the full AdS spacetime (+1 dimension) for gravity. This indicates the existence of a dictionary between the conformal field theory and gravity, i.e. one can make calculations using one of the two theories and have a direct correspondence on the other because they are equivalent [7] :

$$\mathcal{Z}_{gauge} = \mathcal{Z}_{AdS} \tag{19}$$

Gerard 't Hooft's work in the large N expansion [10] hints for a stringy description of QCD. There Gerard 't Hooft realized that only planar diagrams with the quarks at the edges dominate. The ground was set for the so called Holography Principle but it took more than 20 years and the groundbreaking work of Juan M. Maldacena [4] and the realization of D_p branes in string theory by Polchinski (1995) to finally establish the duality in more stable grounds. In other words, with the correspondence two distinct physical theories are equivalent and the way they are equivalent is going to be discussed briefly in this chapter. In more detail, in the first subsection the AdS spacetime is going to be described and motivated. Next, the correspondence is going to be formally described. Finally, we will see how temperature, phase transitions and baryons are implemented in the holographic picture.

3.1 The Anti-de Sitter (AdS) spacetime

As mentioned earlier AdS spacetime in 5 dimensions is ideal to capture the duality due to the local similarity with Minkowski space. It is a spacetime with constant negative curvature. Let us first consider a simpler case [7]. Namely, the AdS_2 spacetime which has SO(2,1) invariance and can be embedded into a flat spacetime with two timelike directions :

$$ds^2 = -dZ^2 - dX^2 + dY^2 \tag{20}$$

$$-Z^2 - X^2 + Y^2 = -L^2 \tag{21}$$

where L is the AdS radius. If we pick the global coordinate system $(\tilde{t}, \rho)$:

$$Z = L\cosh\rho\cos\tilde{t}, \quad X = L\cosh\rho\sin\tilde{t}, \quad Y = L\sinh\rho \tag{22}$$

the metric becomes :

$$ds^2 = L^2(-\cosh^2\rho d\tilde{t}^2 + d\rho^2) \tag{23}$$

We observe that AdS has only one timelike direction $\tilde{t}$ which is periodic with periodicity 2π. In order to avoid problems with causality one has to unwrap the timelike direction and consider the covering space of AdS_2 where $-\infty < \tilde{t} < +\infty$. This spacetime has a constant negative curvature of $R = -\frac{2}{L^2}$. The embedding can be seen in figure 3.

The most common are the static coordinates which can be useful in the comparison with AdS

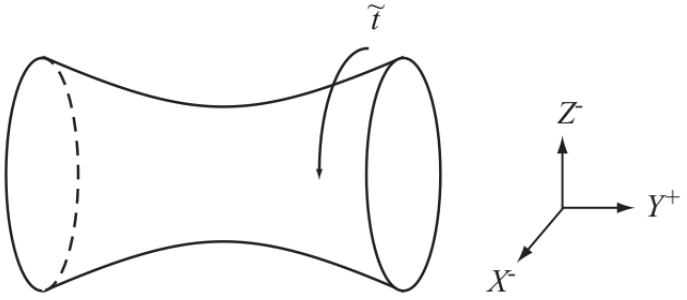

Figure 3: Taken from [7]. Embedding of AdS_2 to $\mathbb{R}^{2,1}$.

black hole, the conformal coordinates where a "spatial" boundary appears and the most widely used Poincaré coordinates. Let's stick to the latter ones a bit further but on higher dimensions.

For $(d > 2)$ they are defined by the following transformations :

$$X_0 = \frac{Lr}{2}(x_i^2 - t^2 + \frac{1}{r^2} + 1) \tag{24}$$

$$X_{p+2} = Lrt \tag{25}$$

$$X_i = Lrx_i, \quad (i = 1, 2, ..., p) \tag{26}$$

$$X_{p+1} = \frac{Lr}{2}(x_i^2 - t^2 + \frac{1}{r^2} - 1) \tag{27}$$

The metric now has the form :

$$\frac{ds^2}{L^2} = r^2(-dt^2 + dx_p^2) + \frac{dr^2}{r^2} \tag{28}$$

where $(r > 0)$ and $(-\infty < t < +\infty)$ and the AdS boundary is located at $r \to \infty$. This metric, which is different from global AdS is also known as the "Poincaré patch". In the AdS/CFT philosophy this boundary condition is used to add external sources to the gauge theory side. When considering the five dimensional AdS for example one can realise its symmetries :

- 4-D Poincaré invariance : this symmetry is enjoyed by x,y,z,t coordinates dual to the gauge theory.
- 4-D scale invariance : transformations of the form $x^\mu \to \alpha x^\mu$ and $r \to \frac{1}{\alpha} r$ leave the metric invariant. The interpretation of the r-coordinate is the gauge theory energy scale.

3.2 Description of AdS/CFT

Hints of AdS/CFT

Before Maldacena who put the correspondence in formal terms there were hints of the duality. More generally, there were hints of a notion that dimensionality plays an important role and that different dimensional theories describing existing physics could be connected. The first hint comes from General relativity when one studies black hole thermodynamics. Black hole entropy is given by the area law [7]:

$$S = \frac{1}{4}\frac{A}{l_{pl}^2}k_B \tag{29}$$

with l_{pl} being the Planck length and is proportional to the area as the name suggests. Although, there is a distinction in this description of entropy as it differs from the thermodynamic entropy in the sense that it does not count the microscopic states and is not proportional to the volume of a system. This is remarkable because it gives us a clue on the nature of black holes microscopic states. There is no correspondence for example of a 4-D black hole to a 4-D statistical system. However, a 5-D area is a 4-D volume. The Holographic Principle describes precisely that. The statistical system which is one dimension lower than the gravitational system is a gauge theory.

The second hint comes from Gerard 't Hooft's work on the large N_c expansion [10], [15]. Trying to tackle QCD non-perturbatively, he considered the limit of large number of colours (N_c) and the theory had two parameters : the number of colours N_c and the gauge theory coupling constant g_{YM}. The 't Hooft coupling is defined as $\lambda = g_{YM}^2 N_c$. The limit is now given by : $N_c \to \infty$ with λ being kept constant and large.

In that limit planar diagrams (4) (diagrams that can be drawn on a plane) dominate suggesting the effect of topology on diagrams. In fact, as the dependence on N goes like N^{2-2h}, where h is the number of "handles", it is clear that diagrams with $h = 0$ dominate in the large N expansion. We see that 2-D diagrams dominate and hence we have a stringy realization of QCD. 't Hooft's work led to the Holographic principle hinting again the connection between two different theories with different dimensionality.

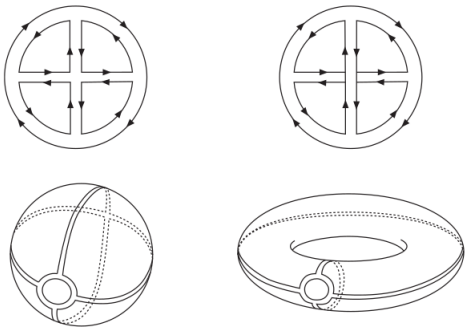

Figure 4: Taken from [15]. A planar diagram that can be drawn on a sphere (left), and a non-planar diagram that must be drawn on a torus (right).

Gubser-Klebanov-Polyakov-Witten (GKPW) relation

The two theories, namely, the one in the bulk and the other on the boundary of the AdS space are related by the following relation [7], [15] :

$$\langle e^{\int d^d x \mathcal{J}(x)\mathcal{O}(x)} \rangle_{CFT} = \int \mathcal{D}\Phi e^{-S_{AdS}}|_{\Phi(x,\partial AdS)=\mathcal{J}(x)} \tag{30}$$

The left hand side (LHS) of this formula describes a 4-D gauge theory in the boundary and the right hand side (RHS) describes a 5-D gravitational theory in the bulk. More precisely, the LHS is the generating functional of the gauge theory with an external source. One can compute there correlators although, things get difficult at strong coupling. However, the RHS is the generating functional of the gravitational theory where at strong coupling (low energy string theory) calculations are easy. A loose description of the procedure done is the following : One usually finds the equations of motion of the field in the bulk Φ but uses the AdS boundary as boundary conditions for the on-shell action S. One acquires a 4-D quantity, namely the boundary value of the source. This way we realize that in general a bulk field in this prescription acts as an external source of a boundary operator. The conversion of calculations made on one side of the duality into the results of calculations on the other side is being done by the so called AdS/CFT "dictionary" [18] :

AdS/CFT Dictionary	
Boundary: field theory	Bulk: gravity
Energy momentum tensor T^{ab}	Metric field g_{ab}
Global symmetry current J^a	Gauge field A_a
Scalar operator O_b	Scalar field Φ
Conformal dimension of the operator	Mass of the field
Source of the operator	Boundary value of the field (leading term)
VEV of the operator	Boundary value of radial momentum of the field (subleading terms)

The dictionary can be generalized to the global aspects of both sides as well [18] :

Global aspects	
Boundary: field theory	Bulk: gravity
Global spacetime symmetry	Local isometry
Temperature	Hawking temperature
Chemical potential/charge density	Boundary values of the gauge potential
Phase transition	thermal gas/black hole solutions

By studying the conformal groups it is shown that the extra dimension r of the bulk is associated with the energy scale of the gauge theory. So when trying to study the UV and IR behaviour of the field theory then one has to study the $r \to \infty$ and $r \to 0$, respectively.

Motivation of AdS/CFT through D-branes

String theory is a theory of strings but also branes. The D-branes are the objects where the endpoints of an open string are constrained. Hence, open strings are on the brane surface but closed strings are free to propagate in the bulk. Since we are interested in QCD which is an

$SU(N_c)$ theory it is important to realize that if we put N_c coincident D-branes the endpoints of open strings have the freedom to be attached to whichever one of the D-branes [7], [17]. This degree of freedom is the correspondence to the $SU(N_c)$ degrees of freedom. D-branes of higher dimensionality are also called Dp-branes where p gives away their dimension. Hence, we will consider a 10-D superstring theory and we will try to mimic QCD. For this, we use a D3-brane which describes a (3+1) gauge theory.

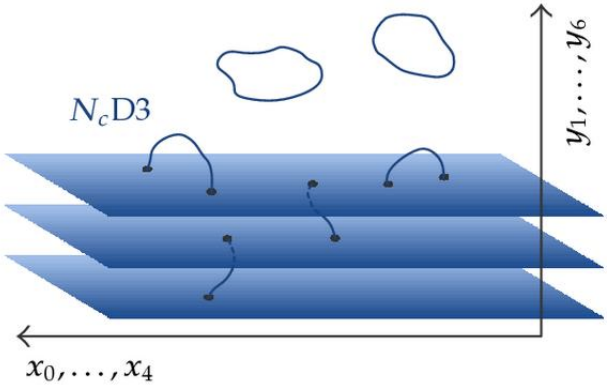

Figure 5: Taken from [17]. Stacked N_c D3-branes in a (9+1) spacetime.

But, in this point we must stress a very important fact. The D3-brane admits two different descriptions at two different scalling limits. So we have two theories for two different limits. In the limit where the string coupling is $g_s \ll 1$ and at the same time $g_s N_c \ll 1$, we get a $\mathcal{N} = 4$ SYM, while for $g_s \ll 1$ and $g_s N_c \gg 1$ we get supergravity on $AdS_5 \times S^5$. In both limits there is a 10-D flat spacetime geometry due to supersymmetry.

More specifically, the D3-brane describes the the 4-D gauge theory that lives in it. But one has to consider extra 6 dimensions due to superstring theory. So, the gauge fields live on the brane and we have a remaining number of 6 scalars that are free to propagate among the branes. These extra fields transform in the adjoint representation of $SU(N_c)$. In the case of D3-branes, we have an isotropy among all the directions for the 6 scalars, which provides us with the so called $SO(2,4) \times SO(6)_R$ symmetry of the $\mathcal{N} = 4$ SYM. So far, we are missing something. D3-branes cannot only describe a gauge theory because they are part of superstring theory that is a unified theory, hence also containing gravity and we are also missing massive string modes.

The mass density of the D-brane according to string theory is :

$$T_3 \simeq \frac{N_c}{g_s}\frac{1}{l_s^4} \tag{31}$$

and also the mass is given by :

$$M \simeq \frac{1}{l_s} \tag{32}$$

So we have to understand how the D-brane affects the geometry. In the first limit mentioned above, one takes $l_s \to 0$ which means that gravity can be ignored (hence the 10-D flat spacetime) and also massive string modes vanish.

It is now fruitful to consider the second limit where l_s is kept finite and $g_s N_c \gg 1$. In this limit, one cannot ignore gravity anymore and the supergravity description of the D-brane becomes more accurate. An observer from infinity does not see anymore a flat space. He rather sees a curved spacetime coming from $u \to 0$. This geometry is described by a black D3-brane solution which reads :

$$ds_{10}^2 = Z^{-\frac{1}{2}}(-dt^2 + dx_3^2) + Z^{\frac{1}{2}}(du^2 + u^2 d\Omega_5^2) \tag{33}$$

$$\text{where} \quad Z = 1 + (\frac{L}{u})^4, \quad L^4 \simeq g_s N_c l_s^4 \tag{34}$$

In the near-horizon limit ($u \ll L$) the metric becomes :

$$ds_{10}^2 \to (\frac{u}{L})^2(-dt^2 + dx_3^2) + L^2(\frac{du^2}{u^2} + d\Omega_5^2) \tag{35}$$

So the geometry is described by $AdS_5 \times S^5$ as advertised in the beginning. Although, away from the source ($u \to 0$) the geometry is still a flat 10-D spacetime, a geometry which is shared in both limits 6.

Summing up, we seem to have two different theories to describe the system at two different regions. AdS/CFT that they are the same since the system doesn't change. In order for this to be true, a calculation must be done somewhere in the middle and the two viewpoints must agree, a task which is not easy and has not been done yet. In the next figure we are going to see the geometry in both limits.
The general form of the correspondence can now be rewritten as [7]: $\mathcal{Z}_{AdS_5} = \mathcal{Z}_{CFT}$.

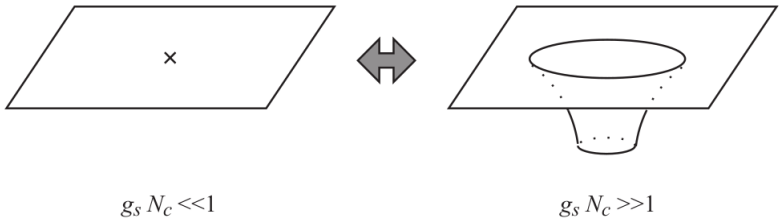

Figure 6: Taken from [7]. In the different limits spacetime can be approximated by either a flat geometry with a source or a curved one.

3.3 Implementation of Temperature and Phase Transitions

In our work, but also in general we are interested in the temperature of a system. For us to use the gauge/gravity duality we must realize how temperature is implemented and connected in both sides. One would say that implementing temperature on the gauge theory side of the correspondence is more intuitive since one can just choose a $SU(N_c)$ theory describing quarks for example and temperature is implemented through the usual statistical mechanics techniques. Although, it is left to see how the temperature in the gravity theory side is associated with the temperature in the gauge theory side. The first step when trying to tackle a gravity problem is to find a solution to the Einstein equations [7].

Fortunately, a solution to Einstein equations with a negative cosmological constant is the Schwarzschild-AdS black hole with a planar horizon. The metric is the following :

$$ds_5^2 = -(\frac{L}{r})^2 h(r) dt^2 + \frac{dr^2}{(\frac{L}{r})^2 h(r)} + (\frac{L}{r})^2 (dx^2 + dy^2 + dz^2) \tag{36}$$

$$\text{where} \quad h(r) = 1 - (\frac{r_0}{r})^4 \tag{37}$$

This metric exhibits an horizon at $r = r_0$ and a curvature singularity at $r = 0$. Planar horizon means that the horizon extends indefinitely in (x, y, z)-directions. Also, this system enjoys scaling symmetries $x^\mu \to \alpha x^\mu$, $r \to \frac{r}{\alpha}$ and $r_0 \to \frac{r_0}{\alpha}$ which means that different black holes arising from this metric have different horizon radii but are in essence, equivalent. In general, the temperature of a black hole is given by the formula :

$$T = \frac{f'(r_0)}{4\pi} \tag{38}$$

and in the current case $T = \frac{1}{\pi}\frac{r_0}{L^2}$. From the area law, one can calculate the entropy density : $s = \frac{S}{V_3} = \frac{1}{4G_5}(\frac{r_0}{L})^3$. Then, by using the temperature and the holographic dictionary from which : $N_c^2 = \frac{\pi}{2}\frac{L^3}{G_5}$, one can arrive at :

$$s = \frac{\pi^2}{2} N_c^2 T^3 \tag{39}$$

and also by making use of $d\epsilon = Tds$, the energy density is given by :

$$\epsilon = \frac{3}{8}\pi^2 N_c^2 T^4 \tag{40}$$

which is a Stefan-Boltzmann law analogue. The AdS radius L and G_5 can be combined to give N_c parameter in the Stefan-Boltzmann law, which is another reason why the Schwarzschild-AdS (S-AdS) black hole is suitable in contrast to the standard Schwarzschild black hole. At this point,

we should also realize the fact that due to the planar horizon giving equivalent systems, no phase transition can be seen. Phase transitions are implemented in our theory via the N_c dependence. When the entropy density is proportional to N_c^2 the dual gauge theory is in the deconfined phase, since entropy basically counts $O(N_c^2)$ degrees of freedom. In the confined phase the entropy density is no longer proportional to N_c^2.

To make a phase transition apparent, we have to use a different solution to the Einstein equations. When using the S-AdS black hole with spherical horizon for example one gets black holes with different horizon radii, creating effectively different systems. emperature is associated by the location of the horizon and horizons now are plenty but different at the same time. Thus, they "create" different systems through the only dimensionful quantity, temperature, which is responsible for phase transitions.

In this thesis we study QCD in the large N_c limit as we will see later. Large N_c gauge theories in general have a rich phase structure as we also saw in the QCD phase diagram [7]. So our new tool, AdS/CFT should provide us with a description of these expected phases, otherwise it has no chance of being realistic. Fortunately, it can be shown that the different phases of interest can be realized by using different solutions that approach AdS asymptotically. The S-AdS black hole with spherical horizon as discussed earlier and also the AdS Soliton solution which has the form :

$$ds_5^2 = (\frac{r}{L})^2(-dt'^2 + dx^2 + dy^2 + hdz'^2) + L^2\frac{dr^2}{hr^2} \tag{41}$$

$$\text{where} \quad L^2 = l\frac{r_0}{\pi} \quad \text{and} \quad h = 1 - (\frac{r_0}{r})^4 \tag{42}$$

This geometry is a compactified $S - AdS_5$ black hole along the z-direction and also "double Wick-rotated". The aforementioned alternations that have occurred, make the geometry to no longer describe an actual black hole because h no longer multiplies time, and also because of the spacetime ending at $r = r_0$. This makes it suitable to describe the confined phase at low temperature $T < \frac{1}{l}$. At high temperature $T > \frac{1}{l}$ one must resort to the S-AdS black hole solution again that describes the plasma phase. At $T = \frac{1}{l}$, a discontinuity occurs at the entropy making apparent a 1st order phase transition from confined to deconfined phase and vice versa.

By parameterizing the theory using TL, one gets for one value of temperature two different values for the horizon location. A "small" and a "large" black hole as is often referred to because they are compared to the AdS scale L. By using these two different horizon locations one

gets two temperatures. Between these two temperatures one has a critical value T_c and when the system is at $T < T_c$ then we have the "thermal gas solution" and when $T > T_c$ we have the "$S - AdS_5$ black hole solution". This also describes the confined/deconfined transition and it is the technique that will appear in our work to describe the different phases as we will see later.

2nd order phase transitions are trickier so we will mention the general idea. For the 1st order phase transition one basically had to change geometries with no black hole to a geometry with compact black hole horizon in order to mimic the discontinuity of the entropy [31]. For the 2nd order one has to change from a black hole geometry to another one which also has a black hole so the entropy is continuous.

3.4 Baryons in SU(N) gauge theory

In this section we are going to describe a picture of how baryons are implemented in the holographic picture. The spirit of this description is consistent with how we are going to treat baryons as well which is the topic of this thesis.

In [21] E. Witten describes baryons in an instructive way using branes. In that context quarks are considered to be the endpoints of Type IIB superstrings in $AdS_5 \times S^5$ which correspond to particles in the fundamental representation of SU(N). These superstrings are supposed to connect two different endpoints x_1 and x_2 in the AdS boundary. If you put N quarks then the endpoints will be $x_1, x_2, x_3, ..., x_N$ and you will have N strings oriented in the same way. The baryon vertex in demand is the point (also named soliton) shown in the figure below (7) where the strings are able to terminate in the bulk of $AdS_5 \times S^5$.

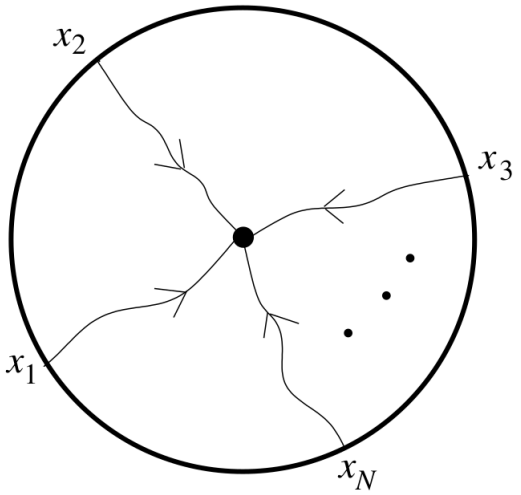

Figure 7: Taken from [21]. A D5-brane couples to N superstrings. In order to cancel out their charge a baryon vertex is produced.

Considering N same external charges in the baryon vertex, one can construct them by wrapping a D5-brane on S^5. In superstring theory there is a self-dual five-form field Ω_5 whose flux on S^5 by N units is given through the $AdS_5 \times S^5$ compactification by :

$$N = \int_{S^5} \frac{\Omega_5}{2\pi} \tag{43}$$

This Ω_5 form is coupled in the worldvolume of the $D_5 - brane$ with a U(1) gauge field α in the

following way :

$$\int_{S^5 \times R} \alpha \wedge \frac{\Omega_5}{2\pi} \tag{44}$$

This produces N-units of charge from the α field. Although, in a closed universe the total charge must be zero, therefore a source must be introduced in the form of the string that has an endpoint in the D5-brane which a gives a total charge of N (+1 or -1 depending on the orientation of the string). So in this case, we need N strings of the same orientation to cancel the N U(1) α charges in the D5-brane. Hence, this point in the D5-brane is the baryon (or antibaryon with an opposite orientation) vertex that we are looking for. Baryons though, are fermions therefore are characterized by antisymmetry. This is achieved by setting proper boundary conditions at spatial infinty but we won't go to such detail here. Other constructions [23], in the same spirit though also apply and will be used in this work. For example, in the case of the D4/D8 model, baryons are identified as D4-branes wrapped on S^4 in the D4 background. Such a D4-brane is realized as a small instanton configuration in the world-volume gauge theory on the probe D8-brane. The main point of this part, is that baryons can indeed be implemented in a string theory picture by considering a five-form which can give us the baryon charge. This will be extremely important in our work because a term like this will be present in the definition of our model and will be used to calculate the baryon charge.

4 AdS/QCD

The goal is to use AdS/CFT in such a way as to describe QCD, its phenomenology and at the same time be in accordance with existing data. So far two approaches are available [22], [31] : the top-down approach and the bottom-up. Both are trying to describe QCD using holography but they use a different path.

Top - down : One starts from a specific string theory set up and the exact dual field theory can be identified. Namely, one uses a D-brane setup in 10-D and then replaces this set-up with a gravitational background of geometry and the various form fields at the "decoupling limit". In the large N_c limit we wish to describe the infrared physics that will strictly specify the correspondence in the duality. This ambitious approach has the great advantage of being extremely precise due to the fact that the field theory is derived. Hence it provides a strict holographic dictionary. Although, this method is extremely difficult as well. The problem rises when considering non-conformal gauge theories on the gauge theory side where there is some low energy scale, like Λ_{QCD} in QCD that breaks conformality and produces Kaluza-Klein (KK) states at the same mass as the states of QCD.

Bottom - up : This method is different from the above. Instead of going all the way from the strict guidelines of the theory where one uses string theory and tries to realize its results, one goes in a more "hand-wavy" way where one implements by hand the operators of interest using some ideas of string theory and tries to write a down a proper action describing the dual fields. In this sense, one builds his way from the bottom, making some necessary assumptions of the components needed, to the top by modelling a specific action which describes a theory like QCD. This action must respect of course the general aspects of the theory under consideration like symmetries, while leaving masses and coupling constants unknown so they can be chosen to fit the data. The next step is to put that action in the test to see how realistic it is with our current data and if yes if it can provide some insights. A variety of bottom-up models have been produced. In this thesis we will work with V-QCD which is an upgraded version of Improved Holographic QCD (IH-QCD) which will be described in short in the next section.

The goal of this chapter is to give a short discussion of the components of the V-QCD bottom-up model on which this work is based on and finally arrive to the V-QCD model and our work.

4.1 Improved Holographic QCD (IH-QCD)

This is the first constituent of the V-QCD model. IH-QCD is modelling the Yang-Mills theory of QCD [31]. It is working on the large N_c limit and is based on a 5-D non-critical string theory involving gravity and a dilaton field $\lambda = e^{\Phi}$ with a non-trivial potential. The action is given by :

$$S_{glue} = M_P^3 N_c^2 \int d^5x \sqrt{-\det g}(R - \frac{4}{3}\frac{(\partial\lambda)^2}{\lambda^2} + V_g(\lambda)) \tag{45}$$

and our ansatz for the metric in the vacuum is the following :

$$ds^2 = e^{2A(r)}(dt^2 + dx^2 + dy^2 + dz^2 + dr^2) \tag{46}$$

The Einstein's equations now take the form :

$$\Phi'^2(r) = -\frac{9}{4}(A''(r) - A'^2(r)), \quad V(\Phi) = e^{2A(r)}(3A''(r) + 9A'^2(r)) \tag{47}$$

The dilaton field e^{Φ} is dual to the TrF^2 operator, so it is identified as the 't Hooft coupling $\lambda = g^2 N_c$ in the gauge theory side which for $\lambda \to \infty$ gives the IR limit and for $\lambda = 0$ gives the UV limit. The r-coordinate is the bulk coordinate and for $r = 0$ we are given the UV boundary which is asymptotically AdS. This metric also possesses a black hole horizon which acts as an IR cutoff breaking conformal symmetry. The $e^{2A(r)}$ is called the conformal factor.

In the UV the metric must be asymptotic to AdS which will provide us with the dilaton dynamics. Additionally, the IR asymptotics of the dilaton potential dictate quark confinement. Hence, we realize that the dilaton potential has to be chosen by hand in the region that is being studied. This signals the fact that this model belongs to the bottom-up family. The background solution of λ is the running coupling constant for QCD. In order for it to be reasonable one has to take into account the restrictions of the physical theory both in UV (large e^{Φ}) and the IR (small e^{Φ}). Usually in the IR limit, the holographic method is to be trusted unlike the UV limit. Hence, for the IR one gets

$$V_g(\Phi) \sim \lambda^{\frac{4}{3}}\sqrt{\log\lambda} \tag{48}$$

so phenomena like confinement, mass gap, discrete spectrum and asymptotically linear glueball trajectories are produced. Since holography is not to be trusted in the UV, one sticks to QCD perturbation theory requiring agreement of the holographic beta function and the perturbative beta function. The potential is then given by :

$$V(\Phi) = \frac{12}{l^2}\left(1 + V_0 e^{\Phi} + V_1 e^{\frac{4}{3}\Phi}[\log(1 + v_2 e^{\frac{4}{3}\Phi} V_3 e^{2\Phi})]^{\frac{1}{2}}\right) \tag{49}$$

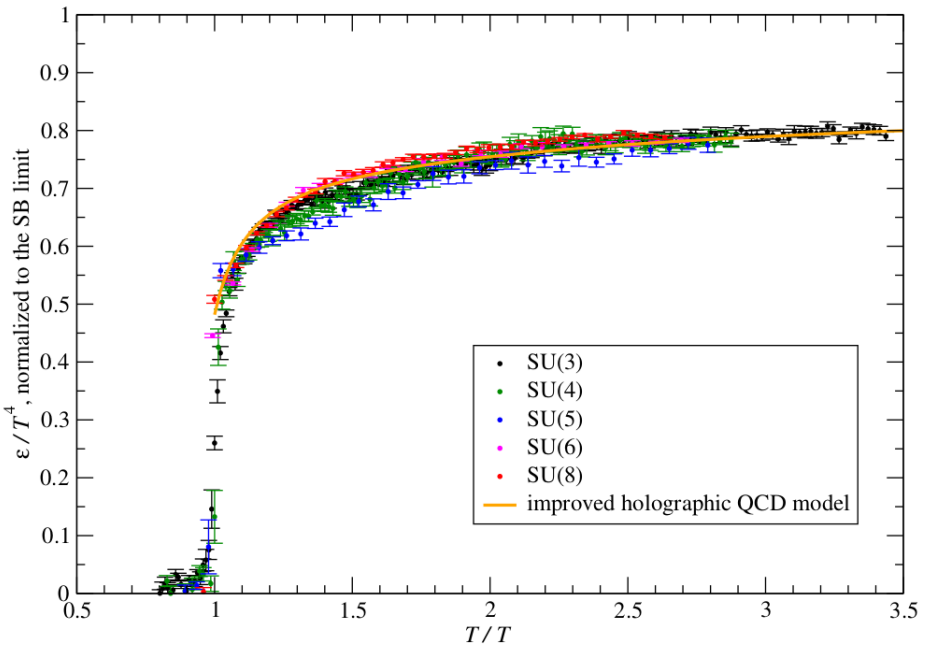

Figure 8: Taken from [32]. Energy density from lattice simulations for different N_c compared with IH-QCD.

which produces a thermal gas phase and two deconfined phases where a "small" and a "big" black hole appear respectively. In the intermediate regions of λ the potentials are coupled through data from experiments and lattice simulations. One last remark is that the IH-QCD model fits surprisingly well with lattice data as we see in the figure 8 of energy density above. We also conclude from the figure that the number of colours N_c do not appear to alter the results. This allows us to consider the large N_c limit as a good qualitative approach of QCD.

4.2 V-QCD setup

V-QCD is the model we are considering in this thesis which is also studied extensively in [11], [16], [22], [29], [37]. More specifically, we want to examine how baryons in the model studied in [3], are affected when a magnetic field is applied. The "V" in the name comes from Veneziano because we are working in the Veneziano limit throughout this model. This means that flavour sector is fully backreacted to the glue sector and we are considering the limits :

$$N_c \to \infty, \quad N_f \to \infty, \quad \frac{N_f}{N_c} \equiv x_f \quad \text{fixed}, \quad g^2 N_c \quad \text{fixed} \tag{50}$$

From the previous section (IH-QCD) we are using the dilaton field $\lambda = e^{\Phi}$ describing the gluonic sector in this manner. But in order for our model to approximate baryons we must also include flavours [29] (i.e. quarks). Flavours are introduced in our model by considering the space being filled with a $D4 - \bar{D}4$ configuration [34] and [14]. We use brane - antibrane pairs by including the physics of an open string tachyon which stretches between the brane - antibrane pairs. In the holographic dictionary the tachyon field is dual to the $\bar{q}q$ operator which is responsible for the chiral symmetry breaking of QCD. On the branes though, live the gauge fields $(A^{\mu}_{L/R})^{ij}$ which are dual to the left and right handed currents $\bar{q}^i \gamma^{\mu}(1 \pm \gamma_5) q^j/2$. The gauge fields A_L, A_R and the tachyon field T are considered in the flavour space, hence they are $N_f \times N_f$ matrices. We also consider the tachyon field to be flavour independent $T = \tau(r)\mathbb{1}_{N_f}$. The gauge fields transform under the left and right $U(N_f)$ as :

$$A_L \to V_L A_L V_L^{\dagger} - i d V_L V_L^{\dagger}, \quad A_R \to V_R A_R V_R^{\dagger} - i d V_R V_R^{\dagger}, \tag{51}$$

$$T \to V_R T V_L^{\dagger}, \quad T^{\dagger} \to V_L T V_R^{\dagger} \tag{52}$$

with $V_L V_L^{\dagger} = \mathbb{1}_{N_f} = V_R V_R^{\dagger}$. The tachyon potential is taken to be Sen-like :

$$V_f(\lambda, TT^{\dagger}) = V_{f_0}(\lambda)^{-\alpha\tau^2} \tag{53}$$

where α is a constant.

The dynamics of a configuration of a stack of N_f brane - antibrane pairs using the tachyon field is captured in the following way :

$$S_{DBI} = -\frac{1}{2} M^3 N_c^2 \mathbb{T}r \int d^5x \left(V_f(\lambda, T^{\dagger}T)\sqrt{-\det \mathbf{A}^{(L)}} + V_f(\lambda, TT^{\dagger})\sqrt{-\det \mathbf{A}^{(R)}} \right) \tag{54}$$

where the radicands are defined as :

$$A^{(L)}_{\mu\nu} = g_{\mu\nu} + w(\lambda, T) F^{(L)}_{\mu\nu} + \frac{\kappa(\lambda, T)}{2} [(D_\mu T)^{\dagger}(D_\nu T) + (D_\nu T)^{\dagger}(D_\mu T)] \tag{55}$$

$$A^{(R)}_{\mu\nu} = g_{\mu\nu} + w(\lambda, T)F^{(R)}_{\mu\nu} + \frac{\kappa(\lambda, T)}{2}[(D_\mu T)(D_\nu T)^\dagger + (D_\nu T)(D_\mu T)^\dagger] \tag{56}$$

The covariant derivative is :

$$D_\mu T = \partial_\mu T + iTA^L_\mu - iA^R_\mu T \tag{57}$$

and the field strength energy tensor is defined by :

$$F^{(L/R)} = dA_{L/R} - iA_{L/R} \wedge A_{L/R} \tag{58}$$

For the model to be complete, the following functions must be specified : $V_g(\lambda), V_{f_0}(\lambda), \kappa(\lambda)$ and $w(\lambda)$. $V_g(\lambda)$ is specified by the IH-QCD, while $V_{f_0}(\lambda), \kappa(\lambda)$ and $w(\lambda)$ are chosen to fit the data. It is important to note that the choice of $w(\lambda)$ is crucial for the baryon physics. The choice of these potentials is dealt in [3]. Finally, the metric ansatz we are using is :

$$ds^2 = e^{2A(r)}(-f(r)dt^2 + dx^2 + dy^2 + e^{2W(r)}dz^2 + f(r)^{-1}dr^2) \tag{59}$$

and the full action of our model using (45) and (54), is summarized in :

$$S_{V-QCD} = S_{glue} + S_{DBI} + S_{CS} \tag{60}$$

where the relevant parts of the final term determine how the solitons source baryonic charge and is going to be explained later.

4.3 Properties of V-QCD

In this section we are going to show some results of V-QCD at finite temperature and chemical potential to see if this model gives indeed some reasonable outcomes so we can continue to our own calculations. In this consideration the bulk fields λ, Φ, T correspond to the three arguments in $p(T, \mu, m_q)$ and only the case where $m_q = 0$ is considered, so the pressure is simply stated as $p(T, \mu)$. By using the same number of massless flavours and colours, namely $x_f = \frac{N_f}{N_c} = 1$, one gets the following dependency of chemical potential with temperature describing the phase transitions [11].

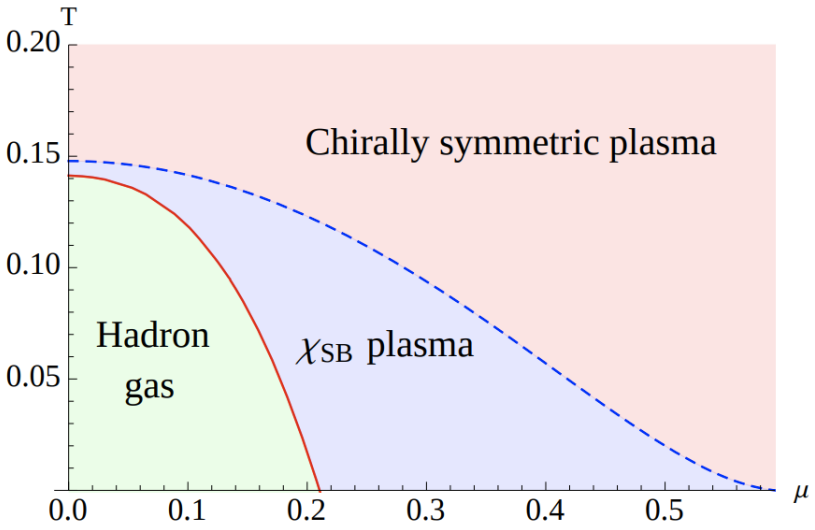

Figure 9: Taken from [11]. Phase transitions in V-QCD at finite temperature. 3 phases are present : hadron gas and 2 plasma phases where chiral symmetry is either broken or restored.

As we can see in figure (9) we have three phases. We must point out that this specific figure has been produced with V-QCD but with a different choice of potentials than the ones we will use in our work. The results though are qualitatively comparable which is why we are considering this figure. For low values of chemical potential and up to intermediate values for temperature we get the "hadron gas", a vacuum phase with zero pressure. For a very small window of temperature which decreases as μ is increased appears a 1st order phase order transition to the broken chiral symmetry plasma phase with a non-zero tachyon. To greater temperatures chiral symmetry is restored in the plasma via a 2nd order phase transition with vanishing tachyon.

The way we get the transitions through pressure in our model is by considering different black hole solutions with dilaton and tachyon hair. It is also worth noting that as $T \to 0$ in the chiral symmetric plasma phase the geometry turn out to be asymptotically $AdS_2 \times \mathbb{R}^3$ making the entropy approach a finite value and not zero. It is speculated to lead to an instability which is assumed to be because of the colours being locked in the Veneziano limit or even the existence of a colour superconducting phase. This structure of the diagram is reasonable when compared to the QCD phase diagram which was introduced earlier, giving us some confidence to consider our model for specific regions in the diagram.

For the vectorial flavour singlet gauge field as : $A_L = A_R = \mathbb{1}_{N_f}\Phi(r)dt$ one gets the following zeroth order DBI action :

$$\begin{aligned} S^{(0)}_{DBI} &= -M^3 N_c N_f \int d^5x V_{f0}(\lambda) e^{-\tau^2} \sqrt{-\det g} \\ &\times \sqrt{(1 + e^{-2A(r)} f(r)\kappa(\lambda)(\tau'(r))^2 - e^{-4A(r)} w(\lambda)^2 (\Phi')^2)} \end{aligned} \tag{61}$$

We should also see what kind of phases does V-QCD actually provide. As usual, we get the different phases by applying different metrics which are the solutions. V-QCD has two solutions. One is the thermal gas solution without a horizon and the other one is a black hole solution with a horizon. Each of these two solution have one extra parameter to take into account that gives rise to an extra phase. This parameter is the existence or not of a scalar tachyon hair, or in simpler words nonzero bulk condensate of the field τ . Its existence or not determines the breaking of the chiral symmetry breaking. With this in mind we can split the phases into four. Although, previous studies [16], [11], [37] with a specific choice for potentials V_g, V_f, κ and w show that only three are relevant :

- Tachyonic thermal gas solution : this is the confined phase of QCD where chiral symmetry is broken for low T and μ.
- Tachyonless black hole solutions : here QCD is deconfined with chiral symmetry restored for large T and μ.
- Tachyonless black hole solutions : in the intermediate values of T and μ this phase might be present depending in the choices for the potentials. Quark matter is deconfined but chiral symmetry is broken. This phase though does not appear in our work.

The above picture can be summarized in the following matrix :

V-QCD phases	
blackening factor $f(r) = 1$	blackening factor $f(r) \neq 1$
Thermal gas with $\tau(r) = 0$	Black hole with $\tau(r) = 0$
Thermal gas with $\tau(r) \neq 0$	Black hole with $\tau(r) \neq 0$

4.4 Turning on Magnetic field and adding baryons in the V-QCD setup

The absence of baryons is realized as the zeroth order of the DBI action and considering the vectorial flavour gauge field with magnetic field (B) turned on as :

$$A_L^M = A_R^M = \left(\Phi(r), -\frac{yB}{2}, \frac{xB}{2}, 0, 0\right) \tag{62}$$

By substituting this choice to calculate the field strength energy tensor (58), also calculate the covariant derivative of the tachyon field (57) and also considering the metric (59) one puts them altogether in (55) and (56) and after that calculates the determinant. In this manner, one gets the zeroth order DBI action :

$$\begin{aligned} S_{DBI}^{(0)} &= -M^3 N_c N_f \int d^5x V_{f_0}(\lambda) e^{-\tau^2} \sqrt{-\det g} \sqrt{(1+e^{-4A(r)}B^2 w(\lambda)^2)} \\ &\times \sqrt{(1+e^{-2A(r)}f(r)\kappa(\lambda)(\tau'(r))^2 - e^{-4A(r)}w(\lambda)^2(\Phi')^2)} \end{aligned} \tag{63}$$

The zeroth order DBI action does not consider the existence of baryons. In order to take them into account they will be added as small perturbations to the gauge field. In this sense we separate the gauge field to Abelian and non-Abelian part :

$$A_L^M = A_R^M = \left(\Phi(r), -\frac{yB}{2}, \frac{xB}{2}, 0, 0\right) + \hat{A}_{L/R}(baryon) \tag{64}$$

The order of the coordinates in the field strength energy tensor is t,x,y,z,r. After plugging in (64), it has the following form :

$$F_{L/R}^{MN} = \begin{pmatrix} 0 & 0 & 0 & 0 & -\Phi'(r) \\ 0 & 0 & B & 0 & 0 \\ 0 & -B & 0 & 0 & 0 \\ 0 & 0 & 0 & 0 & 0 \\ \Phi'(r) & 0 & 0 & 0 & 0 \end{pmatrix} + \hat{F}_{L/R}(baryon)$$

We effectively divide the gauge field into Φ and a flavour singlet part (i.e. the baryon), which is not well defined for generic baryon fields. So we have to impose two consistency conditions to fix this :

$$\begin{aligned} \int d^4x Tr(\hat{F}_{rt}^{(L)} + \hat{F}_{rt}^{(R)}) = 0 \\ \int d^4x Tr(\hat{F}_{xy}^{(L)} + \hat{F}_{xy}^{(R)}) = 0 \end{aligned} \tag{65}$$

Now we move further by developing the radicands (55) and (56) as a series with respect to the small gauge fields :

$$\begin{aligned} A^{(L)}_{MN} &= g_{MN} + \kappa(\lambda)\delta^r_M\delta^r_N(\tau')^2 + w(\lambda)(\delta^r_M\delta^t_N - \delta^t_M\delta^r_N)\Phi' \\ &+ w(\lambda)B(\delta^x_M\delta^y_N - \delta^y_M\delta^x_N) + w(\lambda)F^{(L)}_{MN} + \frac{\kappa(\lambda)\tau^2}{2}(A_MA_N + A_NA_M) \end{aligned} \tag{66}$$

where $A = A_L - A_R$ and a similar identity holds for A^R_{MN}.
The effective metric when neglecting baryons is defined as :

$$\tilde{g} \equiv g_{MN} + \kappa(\lambda)\delta^r_M\delta^r_N(\tau')^2 + w(\lambda)(\delta^r_M\delta^t_N - \delta^t_M\delta^r_N)\Phi' + w(\lambda)B(\delta^x_M\delta^y_N - \delta^y_M\delta^x_N) \tag{67}$$

so that :

$$\begin{aligned} &(\tilde{g}^{-1})^{MP}A^{(L)}_{PN} = (\tilde{g}^{-1})^{MP}\tilde{g}_{PN} + w(\lambda)(\tilde{g}^{-1})^{PN}F^{(L)}_{MN} + \frac{\kappa(\lambda)\tau^2}{2}(\tilde{g}^{-1})^{PN}(A_PA_N + A_NA_P) = \\ &\delta^M_N + w(\lambda)(\tilde{g}^{-1})^{MP}F^{(L)}_{PN} + \frac{\kappa(\lambda)\tau^2}{2}(\tilde{g}^{-1})^{MP}(A_PA_N + A_NA_P) \end{aligned} \tag{68}$$

The way this is expanded is by using $\delta^M_N = 1$ and also setting these two variables :

$$\epsilon_1 K_1 = w(\lambda)(\tilde{g}^{-1})^{MP}F^{(L)}_{PN} \quad \text{and} \tag{69}$$

$$\epsilon_2 K_2 = \frac{\kappa(\lambda)\tau^2}{2}(\tilde{g}^{-1})^{MP}(A_PA_N + A_NA_P) \tag{70}$$

where :

$$\begin{aligned} &\epsilon_1 = w(\lambda), \quad \epsilon_2 = \kappa(\lambda) \quad \text{and} \\ &K_1 = (\tilde{g}^{-1})^{MP}F^{(L)}_{PN}, \quad K_2 = \frac{\tau^2}{2}(\tilde{g}^{-1})^{MP}(A_PA_N + A_NA_P) \end{aligned} \tag{71}$$

And after that we calculate the determinant using the following expansion :

$$\begin{aligned} &\sqrt{det[-(\tilde{g}^{-1})^{MP}A^{(L)}_{PN}]} = \sqrt{det(1+\epsilon K)} = e^{Tr(log1+\epsilon K)} = \\ &e^{Tr(\epsilon K - \frac{1}{2}\epsilon^2K^2)+\dots} = 1 + Tr(\epsilon K) - \frac{1}{2}Tr(\epsilon K)^2 + \frac{1}{2}(Tr\epsilon K)^2 + \dots \end{aligned} \tag{72}$$

The order of coordinates is again t,x,y,z,r and the effective metric $\tilde{g}^{MP}$ has the form :

$$\begin{pmatrix} -e^{2A(r)}f(r) & 0 & 0 & 0 & -w(\lambda)\Phi'(r) \\ 0 & e^{2A(r)} & Bw(\lambda) & 0 & 0 \\ 0 & -Bw(\lambda) & e^{2A(r)} & 0 & 0 \\ 0 & 0 & 0 & e^{2A(r)+2W(r)} & 0 \\ w(\lambda)\Phi'(r) & 0 & 0 & 0 & \frac{e^{2A(r)}}{f(r)} + \kappa(\lambda)(\tau')^2 \end{pmatrix}$$

and the inverse $(\tilde{g}^{-1})^{MP}$ is :

$$\begin{pmatrix} \frac{-e^{2A(r)}+e^{-8A(r)}(e^{4A(r)}+B^2w(\lambda)^2)\kappa(\lambda)f(r)(\tau')^2}{f(r)\Xi} & 0 & 0 & 0 & -\frac{e^{-4A(r)}(1+B^2w(\lambda)^2e^{-4A(r)})w(\lambda)\Phi'(r)}{\Xi} \\ 0 & \frac{e^{2A(r)}}{e^{4A(r)}+B^2w(\lambda)^2} & \frac{-Bw(\lambda)}{e^{4A(r)}+B^2w(\lambda)^2} & 0 & 0 \\ 0 & \frac{Bw(\lambda)}{e^{4A(r)}+B^2w(\lambda)^2} & \frac{e^{2A(r)}}{e^{4A(r)}+B^2w(\lambda)^2} & 0 & 0 \\ 0 & 0 & 0 & e^{-2A(r)-2W(r)} & 0 \\ \frac{e^{-4A(r)}(1+B^2w(\lambda)^2e^{-4A(r)})w(\lambda)\Phi'(r)}{\Xi} & 0 & 0 & 0 & \frac{e^{2A(r)}(1+B^2w(\lambda)^2e^{-4A(r)})f(r)}{\Xi} \end{pmatrix}$$

with Ξ being defined as :

$$\begin{aligned} &\Xi = \frac{det\tilde{g}}{detg} = \\ &(1+e^{-4A(r)}B^2w(\lambda)^2)\bigg(1+e^{-2A(r)}\kappa(\lambda)f(r)(\tau')^2 - e^{-4A(r)}w(\lambda)^2(\Phi')^2\bigg) \end{aligned} \tag{73}$$

We now calculate the following term as it will be important for the calculation of $\sqrt{-detA^{(L/R)}}$:

$$(\tilde{g}^{-1})^{MN}F^{(L)}_{NM} = \frac{2w(\lambda)\Phi'}{\zeta}F^{(L)}_{tr} + \frac{2Bw(\lambda)}{e^{4A(r)}+B^2w^2(\lambda)}F^{(L)}_{xy} \tag{74}$$

where $\zeta = e^{4A(r)} + e^{2A(r)}f(r)\kappa(\lambda)(\tau')^2 - w(\lambda)^2(\Phi')^2$.

We can now write down the expression for the determinant :

$$\begin{aligned} &\sqrt{-detA^{(L/R)}} = \sqrt{-det\tilde{g}}\bigg(1+\frac{w(\lambda)}{2}\bigg(2w(\lambda)\Phi'F^{(L/R)}_{tr}\Xi^{-1}e^{-8A(r)}(e^{4A(r)}+B^2w(\lambda)^2+ \\ &\frac{2Bw(\lambda)}{e^{4A(r)}+B^2w(\lambda)^2}F^{(L/R)}_{xy}\bigg) + \frac{\kappa(\lambda)\tau^2}{2}(\tilde{g}^{-1})^{MN}_s\mathbb{T}rA_MA_N \\ &-\frac{w(\lambda)^2}{4}\mathbb{T}r\bigg((\tilde{g}^{-1})^{MN}_sF^{(L)}_{NP}(\tilde{g}^{-1})^{PQ}_sF^{(L/R)}_{QM}\bigg)\bigg) \end{aligned} \tag{75}$$

At this point we are able to substitute this expression in the DBI action (54) in order to get the leading order term which icludes the zeroth order term $(S^{(0)}_{DBI})$:

$$\begin{aligned} &S^{(1)}_{DBI} = -M^3N_cTr\int d^5xV_{f0}(\lambda)e^{-\tau^2}\sqrt{-det\tilde{g}}\bigg(1+\frac{w^2(\lambda)}{2}\Phi'\Xi^{-1}e^{-8A(r)}(e^{4A(r)} \\ &+B^2w^2(\lambda))(F^{(L)}_{tr}+F^{(R)}_{tr}) + \frac{Bw^2(\lambda)}{2(e^{4A(r)}+B^2w^2(\lambda))}(F^{(L)}_{xy}+F^{(R)}_{xy}) \\ &+\frac{\kappa(\lambda)\tau^2}{2}(\tilde{g}^{-1})^{MN}A_MA_N - \frac{w^2(\lambda)}{8}(\tilde{g}^{-1})^{MN}_s(\tilde{g}^{-1})^{PQ}_s(F^{(L)}_{NP}F^{(L)}_{QM}+F^{(R)}_{NP}F^{(R)}_{QM})\bigg) \end{aligned} \tag{76}$$

By applying the consistency conditions (65) the action gets the final form :

$$\begin{aligned} &S^{(1)}_{DBI} = -M^3N_cTr\int d^5xV_{f_0}(\lambda)e^{-\tau^2}\sqrt{-det\tilde{g}}\sqrt{\Xi}\bigg(\frac{\kappa(\lambda)\tau^2}{2}(\tilde{g}^{-1})^{MN}\mathbb{T}rA_MA_N \\ &-\frac{w(\lambda)^2}{8}(\tilde{g}^{-1})^{MN}_s(\tilde{g}^{-1})^{PQ}_s\mathbb{T}r(F^{(L)}_{NP}F^{(L)}_{QM}+F^{(R)}_{NP}F^{(R)}_{QM})\bigg) \end{aligned} \tag{77}$$

4.5 Chern - Simons terms

In the full action of the V-QCD model (60) we saw that the first term is responsible for the behaviour of gluons and the DBI term is the realization of flavours through branes. The model though also consists of a third term, namely S_{CS}, where CS stands for Chern - Simons. This term is crucial for our work, since via this term we will be able to identify the total baryon number N_b and calculate the baryon charge ρ by making a specific approach which will be explained in the next section. The 5-form Ω_5 which appears in the definition of the S_{CS} is responsible for the baryon vertex in a similar manner as was discussed in section 3.4 and the quantities that we mentioned above are going to be calculated via the coupling of Φ, B and f_B (which will be defined below). The S_{CS} term has been studied extensively in [33] and the form Ω_5 that we will use is explained also in [14], so in this work we will merely use their results and follow their reasoning.

In these terms appears a potential $V_\alpha(\lambda, \tau)$ which has some constraints. In the UV ($\lambda = \tau = 0$) its normalization must reproduce the correct axial anomaly and perturbative corrections in λ must vanish due to the perturbative nonrenormalization of the anomaly. Also, in the IR the contributions from the CS terms have to vanish faster than those coming from the DBI. So the string motivated ansatz is the following : $V_\alpha(\lambda, \tau) = e^{-b\tau^2}$ for $b > 1$. Although, we are going to set $b = 1$ for simplicity and it is going to be reintroduced later through τ.

The relevant term is given by [14] and is :

$$S_{CS} = \frac{iN_c}{4\pi^2} \int \Omega_5 \tag{78}$$

where

$$\begin{aligned}\Omega_5 = \frac{1}{6}\mathbb{T}re^{-\tau^2}\Bigg(& -iA_L\wedge F^{(L)}\wedge F^{(L)} + \frac{1}{2}A_L\wedge A_L\wedge A_L\wedge F^{(L)} \\ & + \frac{i}{10}A_L\wedge A_L\wedge A_L\wedge A_L\wedge A_L + iA_R\wedge F^{(R)}\wedge F^{(R)} - \frac{1}{2}A_R\wedge A_R\wedge A_R\wedge F^{(R)} \\ & - \frac{i}{10}A_R\wedge A_R\wedge A_R\wedge A_R\wedge A_R + \tau^2\big[iA_L\wedge F^{(R)}\wedge F^{(R)} - iA_R\wedge F^{(L)}\wedge F^{(L)} \\ & + \frac{i}{2}(A_L - A_R)\wedge(F^{(L)}\wedge F^{(R)} + F^{(R)}\wedge F^{(L)}) + \frac{1}{2}A_L\wedge A_L\wedge A_L\wedge F^{(L)} \\ & - \frac{1}{2}A_R\wedge A_R\wedge A_R\wedge F^{(R)} + \frac{i}{10}A_L\wedge A_L\wedge A_L\wedge A_L\wedge A_L \\ & - \frac{i}{10}A_R\wedge A_R\wedge A_R\wedge A_R\wedge A_R\big] \\ & + i\tau^3 d\tau\wedge\big[(A_L\wedge A_R - A_R\wedge A_L)\wedge(F^{(L)} + F^{(R)}) + iA_L\wedge A_L\wedge A_L\wedge A_R \\ & - \frac{i}{2}A_L\wedge A_R\wedge A_L\wedge A_R + iA_L\wedge A_R\wedge A_L\wedge A_R\big] \\ & + \frac{i}{20}\tau^4(A_L - A_R)\wedge(A_L - A_R)\wedge(A_L - A_R)\wedge(A_L - A_R)\wedge(A_L - A_R)\Bigg)\end{aligned} \tag{79}$$

Following the work of [3] we want to extract the coupling between the solitonic components, Φ, f_B and B by substituting $A_{L/R} \to \Phi dt - \frac{yB}{2}dx + \frac{xB}{2}dy + A_{L/R}$ and after that collect the coupling terms. For simplicity of calculations we have introduced the term $f_B = -\frac{y}{2}dx + \frac{x}{2}dy$ and we also add two total derivative terms (which are given in the appendix) to get to :

$$\tilde{\Omega}_5 = \Omega_{5\,\Phi=0} + \frac{1}{30}\Phi dt\wedge H_4^{(\Phi)} + \frac{1}{30}Bf_B\wedge H_4^{(B)} + \frac{1}{30}B\Phi dt\wedge df_B\wedge H_2 \tag{80}$$

where

$$\begin{aligned}e^{\tau^2}H_4^{(\Phi)} = \mathbb{T}r\Bigg(& -3iF^{(L)}\wedge F^{(L)} + 3iF^{(R)}\wedge F^{(R)} + 6i\tau d\tau\wedge(A_L - A_R)\wedge(F^{(L)} + F^{(R)}) \\ & + 3\tau^2(A_L - A_R)\wedge(A_L - A_R)\wedge(F^{(L)} - F^{(R)}) \\ & + \tau^3 d\tau\wedge(-4iA_L\wedge F^{(R)} + 4iA_R\wedge F^{(L)} + A_R\wedge A_L\wedge A_L \\ & - 2A_R\wedge A_R\wedge A_L - 2A_L\wedge A_L\wedge A_L + 2A_R\wedge A_R\wedge A_R)\Bigg)\end{aligned} \tag{81}$$

The additional terms that appear in (80) are another 4-form $H_4^{(B)}$ and a 2-form H_2 whose full form is similar to (81) and are going to be given explicitly in the appendix. In this calculation the following exterior algebra rules for the forms were applied :

- $f_B\wedge f_B = (-ydx + xdy)\wedge(-ydx + xdy) = 0$
- $d\tau\wedge d\Phi = 0$

- $df_B \wedge df_B = (2dx \wedge dy) \wedge (2dx \wedge dy) = 0$
- $d\tau \wedge f_B = (\partial_\mu \tau dx^\mu) \wedge (-ydx + xdy) = -y\partial_r \tau(r) dr \wedge dx + x\partial_r \tau(r) dr \wedge dy$
- $d\Phi \wedge df_B = (\partial_\mu \Phi dx^\mu) \wedge (2dx \wedge dy) = 2\partial_r \Phi(r) dr \wedge dx \wedge dy$
- $f_B \wedge df_B = 0$
- $d\tau \wedge df_B = (\partial_\mu \tau dx^\mu) \wedge (2dx \wedge dy) = 2\partial_r \tau(r) dr \wedge dx \wedge dy$
- $d\Phi \wedge f_B = -y\partial_r \Phi(r) dr \wedge dx + x\partial_r \Phi(r) dr \wedge dy$

By applying these rules and imposing our homogeneous ansatz (as is going to be explained later) on the derivative terms of $H_4^{(B)}$ and H_2, we see that $f_B \wedge H_4^{(B)}$ and $dt \wedge df_B \wedge H_2$ evaluate to zero. This is not the case for $dt \wedge H_4^{(\Phi)}$. It is closed and exact, $dH_4^{(\Phi)} = 0$. Hence, we move on taking into account only the term $H_4^{(\Phi)}$ which is :

$$
\begin{aligned}
e^{\tau^2} \Phi \wedge H_4^{(\Phi)} = \mathbb{T}r\Big(& -15i\Phi \wedge F^{(L)} \wedge F^{(L)} + 15i\Phi \wedge F^{(R)} \wedge F^{(R)} + 15\tau^2 \Phi \wedge A_L \wedge A_L \wedge F^{(L)} \\
& - 15\tau^2 \Phi \wedge A_L \wedge A_L \wedge F^{(R)} - 15\tau^2 \Phi \wedge A_L \wedge A_R \wedge F^{(L)} + 15\tau^2 \Phi \wedge A_L \wedge A_R \wedge F^{(R)} \\
& + 15\tau^2 \Phi \wedge A_L^T \wedge A_R^T \wedge F^{(L)T} - 15\tau^2 \Phi \wedge A_L^T \wedge A_R^T \wedge F^{(R)T} + 15\tau^2 \Phi \wedge A_R \wedge A_R \wedge F^{(L)} \\
& - 15\tau^2 \Phi \wedge A_R \wedge A_R \wedge F^{(R)} + 8i\Phi \wedge A_L \wedge A_L \wedge A_L \wedge A_L + 8i\tau^2 \Phi \wedge A_L \wedge A_L \wedge A_L \wedge A_L \\
& - 8i\Phi \wedge A_R \wedge A_R \wedge A_R \wedge A_R - 8i\tau^2 \Phi \wedge A_R \wedge A_R \wedge A_R \wedge A_R + 30i\tau\Phi \wedge d\tau \wedge A_L \wedge F^{(L)} \\
& + 30i\tau\Phi \wedge d\tau \wedge A_L \wedge F^{(R)} - 30i\tau\Phi \wedge d\tau \wedge A_R \wedge F^{(L)} - 30i\tau\Phi \wedge d\tau \wedge A_R \wedge F^{(R)} \\
& - 10\tau^3 \Phi \wedge d\tau \wedge A_L \wedge A_L \wedge A_L + 30\tau^3 \Phi \wedge d\tau \wedge A_L \wedge A_L \wedge A_R \\
& - 30\tau^3 \Phi \wedge d\tau \wedge A_L \wedge A_R \wedge A_R + 10\tau^3 \Phi \wedge d\tau \wedge A_R \wedge A_R \wedge A_R \Big)
\end{aligned}
\tag{82}
$$

The total charge density is defined as :

$$
\rho = -\frac{\delta S_{V-QCD}}{\delta \Phi'}|_{bdry} = \int dr \frac{\delta S_{V-QCD}}{\delta \Phi} \tag{83}
$$

where the equations of motion for Φ are used, which is why the baryon charge is given by the coupling to Φ in the CS action :

$$
N_c N_b = \int dr d^3x \frac{\delta S_{CS}}{\delta \Phi} = \frac{iN_c}{24\pi^2} \int H_4^{(\Phi)} \tag{84}
$$

with N_b being the total baryon number. At this point it becomes clear that the integral above includes non-Abelian terms $(A_L, A_R, F^{(L)}, F^{(R)})$ that we do not know how to substitute. Our

idea is to use an approximations for these terms in order to include baryons. This approximation will attempt to describe them in a specific way so we can continue with our calculations. For this to be achieved an ansatz is going to be made, which is motivated the next section.

5 Baryons from a homogeneous bulk gauge field in V-QCD

Before jumping into the calculations we should first analyze the idea of baryons in general and then the approximation which will be used. Our goal is to realize how the magnetic field affects the baryons in the context of cold QCD described by V-QCD. Historically, baryons are being included in top-down approaches in various ways. A D-brane that joins N_c open strings gives a baryon vertex and the baryon number is provided through the Chern-Simons terms by the coupling of a five-form as discussed earlier. In effective holographic theories though, baryons have been implemented using the Witten-Sakai-Sugimoto (WSS) top-down model [23], in which they were approached as small solitons in the beginning and then it was generalized to include contributions beyond this approach. When one tries to be more specific, namely wants to study baryons for high values of μ_b and low T in the QCD phase diagram, homogeneous approximations have been made before in the WSS model but also in probe branes. In terms of the holographic dictionary, one can see that dense baryonic QCD matter is dual to configurations with a high density of solitons so it makes sense to

The way we are going to approach the baryons in this work is the following. To simplify the analysis we will consider the baryon configuration to be homogeneous in spatial directions, working also in an isospin symmetric setup neglecting the effects due to light quark masses. Our ansatz enjoys a SU(2) flavour symmetry in the spatial components of the non-Abelian flavour gauge field and it is on top of a fixed thermal gas gravitational backgound. The baryon density is given again from the Chern-Simons terms. The whole bulk will be filled with the homogeneous baryon field $h(r)$ (system with a high density of baryons), but there will be a region that the solution there is highly inhomogeneous and will be modeled through a discontinuity. One can also see this in the superstring theory picture. Namely, the whole bulk is filled in a homogeneous way with N $D_4 - branes$ with each one giving a baryon charge because of their coupling. We are assuming that the baryon (or soliton) centers are at some point r_c. This specific point is hard to solve analytically. So what we are doing is that we assume that there is a localized discontinuity of the $h(r)$ field at a very specific and narrow "line" at r_c which since we consider small we don't take it into account. The baryon field though in the rest of the bulk is homogeneous, giving us the impression of having "tails" for each soliton. In this context we can solve for equations of motion for the rest of the bulk by varying with respect to r_c and minimizing the action there. Hence, in the r-direction there will be three regions splitted by the "soliton centers" in r_c :

- $r \ll r_c$: the region close to the boundary is well described by the homogeneous baryon field.
- $r \sim r_c$: here is where the discontinuity lies making the configuration highly inhomogeneous and nontrivial.
- $r \gg r_c$: the region close to the IR is again well described by the homogeneous baryon field.

This can also be seen graphically in the following drawing (10) :

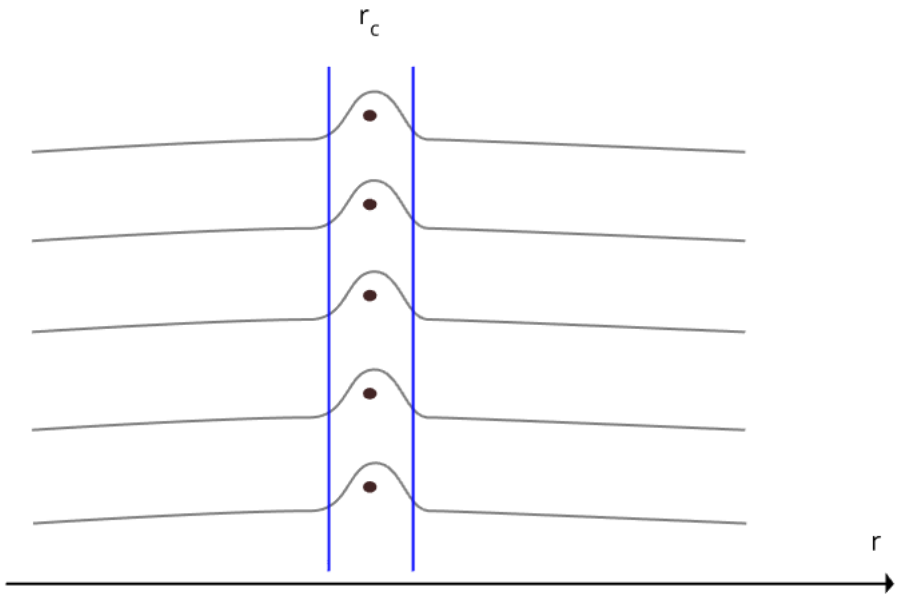

Figure 10: Homogeneous ansatz, where we assume that soliton centers are located in a narrow highly inhomegeneous area but the rest of space is homogeneous.

One can safely assume in this context that when the density of baryons is taken to be very high, like in our case, then the small area that produces the inhomogeneity in the middle of the bulk should not affect the main characteristics of the QCD phase diagram.

5.1 Setup

At this point we will introduce our ansatz which will be plugged into the DBI action that is known only up to first order for non-Abelian gauge fields and also the Chern-Simons part of the action. The ansatz is SU(2) solitons in the thermal gas background, namely the non-Abelial part of the gauge field which respects chiral symmetry and parity [19], [20] :

$$A_L^i = -A_R^i = h(r)\sigma^i \tag{85}$$

In order to get the baryon charge we must calculate $\int dt \wedge H_4^{(\Phi)}$:

$$\int dt \wedge H_4^{(\Phi)} = 48i \int d^5x \frac{d}{dr}[e^{-b\tau^2(r)}h^3(r)(1-2b\tau^2(r))] \tag{86}$$

where the coefficient b has been rescaled back in τ and $h(r)$ is the baryon field. The problem is that the UV and IR contributions vanish giving us zero total derivative boundary terms and baryon density. More specifically, the tachyon sets the action to zero in the IR and $h(r)$ vanishes in the UV. The way to come around is through the discontinuity of $h(r)$ in the region in between which gives nonzero baryon density. Plugging in the ansatz in $S_{DBI}^{(1)}$ and considering S_{CS} we get the full action :

$$\begin{aligned}
&S_h = S_{DBI}^{(0)} + S_{DBI}^{(1)} + S_{CS} = \\
&-2M^3N_c \int d^5x V_{f_0}(\lambda) e^{-\tau(r)^2} e^{5A(r)+W(r)} \sqrt{\Xi} \Bigg(1 + \frac{2e^{-4A(r)-2W(r)}(e^{2W(r)}+2Q^2)w(\lambda)^2h^4(r)}{Q^4} \\
&+ \frac{2e^{-2A(r)-2W(r)}(2e^{2W(r)}+Q^2)\tau^2\kappa(\lambda)h^2(r)}{Q^2} + \frac{e^{-4A(r)-2W(r)}(2e^{2W(r)}+Q^2)w(\lambda)^2f(r)h'(r)^2}{2\Xi} \Bigg) \\
&-\frac{2N_c}{\pi^2} \int d^5x \frac{d}{dr}[e^{-b\tau^2(r)}h^3(r)(1-2b\tau^2(r))]
\end{aligned} \tag{87}$$

where Ξ when introducing (88) has the form : $\Xi = Q^2\big(G^2 - e^{-4A(r)}w(\lambda)^2(\Phi')^2\big)$.
Also:

$$\begin{aligned}
Q^2 &= 1 + w(\lambda)^2 B^2 e^{-4A(r)} \\
G^2 &= 1 + e^{-2A(r)} f(r)\kappa(\lambda)(\tau(r)')^2
\end{aligned} \tag{88}$$

The action we just presented is trusted only far away from $r = r_c$, where $h(r)$ is not discontinuous. We ignore the singular contributions that arise from the $h'(r)$ terms by treating the our integrals in the following manner :

$$\int_0^\infty dr \to \left(\int_0^{r_c^-} + \int_{r_c^+}^\infty \right) dr \equiv \lim_{\epsilon \to 0+} \left(\int_0^{r_c-\epsilon} + \int_{r_c+\epsilon}^\infty \right) dr \tag{89}$$

From this action (87) the charge density can be derived. Note that there is a Φ' dependency in Ξ. So:

$$\rho = -\frac{\delta S_h}{\delta \Phi'} = -\frac{V_\rho e^{W(r)} e^{-4A(r)} Q^2 w^2 \Phi'}{\sqrt{\Xi}} \tag{90}$$

where

$$V_\rho = 2M^3 N_c V_{f_0}(\lambda) e^{-\tau(r)^2} e^{5A(r)} \tag{91}$$

The only part of the full action depending on Φ is the S_{cs} term. Hence, using the Φ equation of motion we have :

$$\rho' = -\frac{d}{dr}\frac{\delta S_h}{\delta \Phi'} = -\frac{\delta S_h}{\delta \Phi} = \frac{2N_c}{\pi^2}\frac{d}{dr}[e^{-b\tau^2} h^3(1-2b\tau^2)] \tag{92}$$

except again the point $r = r_c$ where h is discontinuous. Also, for ρ :

$$\rho = \begin{cases} \varrho + \frac{2N_c}{\pi^2}[e^{-b\tau^2} h^3(1-2b\tau^2)], (r < r_c) \\ \\ \frac{2N_c}{\pi^2}[e^{-b\tau^2} h^3(1-2b\tau^2)], (r > r_c) \end{cases}$$

where ϱ is the density at the boundary (i.e. the physical baryon density) and can be written in terms of the discontinuity :

$$\varrho = \frac{2N_c}{\pi^2} e^{-b\tau(r_c)^2}(1-2b\tau(r_c)^2)\,\mathrm{Disc}\, h^3(r_c) \tag{93}$$

where the discontinuity is defined as :

$$\mathrm{Disc}\, g(r) \equiv \lim_{\epsilon \to 0+} \Big(g(r+\epsilon) - g(r-\epsilon) \Big) \tag{94}$$

Our goal for future work is to introduce a more generalized and sophisticated anstatz. This is the following :

$$\begin{aligned} A_L^1 &= -A_R^1 = h(r) g(r) \sigma^1 \\ A_L^2 &= -A_R^2 = h(r) g(r) \sigma^2 \\ A_L^3 &= -A_R^3 = \frac{h(r)}{g^2(r)} \sigma^3 \end{aligned} \tag{95}$$

We know use a more generalized function in the direction of the magnetic field and the goal is to perform the same numerical analysis as will be done later and conclude whether we can

indeed generalize this ansatz or not. This specific ansatz is not worked out fully yet. However, we have plugged it in the Chern - Simons terms introduced in the previous chapter and the result is encouraging. An analogue to (86) is the following by performing the same calculations but using (95) this time :

$$\int dt \wedge H_4^{(\Phi)} = 48i \int d^5x \frac{d}{dr}[e^{-b\tau^2(r)}(h^3(r) - 2h^3(r)b\tau^2(r))] \tag{96}$$

This is a good result because the baryon charge can still be written in terms of a total derivative. This allows us to continue further in the numerical analysis. We will not consider this ansatz in the rest of this thesis, though. We will only work with (85) from now on.

5.2 Grand potential

In this section follows the calculation of the Grand potential. According to our approximation, solitons exist at the discontinuity located at r_c. We are going to find that specific point by minimizing the action that we derived above while keeping the physical baryon density fixed. A soliton in the r-direction in the CS term can be written as :

$$S_{CS} \simeq \frac{iN_c}{24\pi^2}\Phi(r_b)\int dt \wedge H_4^{(\Phi)} \tag{97}$$

This is true because the other forms $H_4^{(B)}$ and H_2 evaluate to zero at the homogeneous ansatz that we are considering. Moreover, we can see that field Φ is simply coupled leading us to baryons carrying a fixed charge. Hence, we consider ϱ in (93) fixed. Since also $H_4^{(\Phi)}$ is exact, the integral becomes a boundary term, which suggests that the quantization can be read off by inserting the asymptotic form of the soliton solution in this expression. This leads the discontinuity to diverge at r_c being too deep in the IR and also at r_c where $2b\tau^2(r_c)^2 = 1$. The free energy and the DBI action diverge as well at this point preventing the baryon from falling in the IR. Another fact that comes up when considering fixed charge baryons, is that we should work on the canonical ensemble by performing a Legendre transformation :

$$\tilde{S}_h = S_h - \int d^4x\Phi(0)\rho(0) = S_h + \int d^5x\frac{d}{dr}[\Phi\rho] \tag{98}$$

and since at $r = r_c$ the CS terms become : $S_{cs} = \int d^5x\Phi\rho'$ we get :

$$\tilde{S}_h = S_{DBI} + \int d^5x\Phi'\rho \tag{99}$$

The next step is to find Φ' by inverting the charge density (90) and plugging it into (99). There is a little trick to get Φ' expression. Namely, we should recall that we are working in an expansion of the original DBI action at small amplitudes of $F^{(L/R)}$. So when expanding to get Φ' we ignore higher powers of h. After considering all this we have :

$$\begin{aligned}\Phi' = &-\frac{e^{4A(r)}G\rho}{w\sqrt{e^{2W(r)}Q^2V_\rho^2w^2 + e^{4A(r)}\rho^2}}\Bigg(1 - \frac{2e^{-4A(r)}(e^{2W(r)} + 2Q^2)V_\rho^2w^4h^4(r)}{Q^2(e^{2W(r)}Q^2V_\rho^2w^2 + e^{4A(r)}\rho^2)} \\ &- \frac{2e^{-2A(r)}(2e^{2W(r)} + Q^2)V_\rho^2w^2\tau^2\kappa(\lambda)h^2(r)}{e^{2W(r)}Q^2V_\rho^2w^2 + e^{4A(r)}\rho^2} + \frac{e^{-4A(r)-2W(r)}(2e^{2W(r)} + Q^2)w^2f(r)h'^2(r)}{2G^2Q^2}\Bigg)\end{aligned} \tag{100}$$

Now we can write down the final action where Q and G are defined in (88) and V_ρ in (91) :

$$\tilde{S}_h = -\int d^5x V_\rho G \sqrt{e^{2W(r)}Q^2 + \frac{\rho^2}{(V_\rho w e^{-2A(r)})^2}}\Bigg(1 + \frac{2e^{4A(r)}(e^{2W(r)}+2Q^2)V_\rho^2 w^4 h^4(r)}{Q^2(e^{2W(r)}Q^2V_\rho^2w^2+e^{4A(r)}\rho^2)} + \frac{2e^{-2A(r)}(2e^{2W(r)}+Q^2)V_\rho^2 w^2\tau^2\kappa(\lambda)h^2(r)}{e^{2W(r)}Q^2V_\rho^2w^2+e^{-4A(r)}\rho^2} + \frac{e^{-4A(r)-2W(r)}(2e^{2W(r)}+Q^2)w^2 f(r)h'^2(r)}{2G^2Q^2}\Bigg) \tag{101}$$

Numerical analysis

From these equations we are now able to extract the Lagrangian and then calculate the equations of motion for $h(r)$. They admit two types of solutions, namely black hole and thermal gas solutions. For our numerical analysis, we need to construct the confining background first (the metric and the scalars) which is generated by shooting from the IR. This is achieved by considering the equations of motion and boundary conditions of the background fields A, f, λ, and τ [3]. Then we insert the background in (101) and we solve the resulting equations of motion for $h(r)$. This numerical procedure has been done before and is explained in detail in [11]. We have to get rid of the divergences that appear in the action though. These exist in the dilaton gravity part and in the zeroth order DBI action $S^{(0)}_{DBI}$ (i.e. thermal gas background). We do not perform a regularization in the standard manner. We rather evaluate the difference between the full baryon action $\tilde{S}_h$ and the thermal gas background with zero baryon charge $S^{(0)}_{DBI}$. In this way, the divergences cancel trivially and exactly against the same terms for the reference solution i.e. the thermal gas background.

The location of r_c is computed numerically and not analytically as well. The way this is achieved is by minimizing the action we derived with respect to r_c and C_2. C_2 is the free parameter rising through the asymptotics of the $h(r)$ field that we introduced via our ansatz. In more detail, we insert the standard UV behaviour and solving for $h(r)$ we get the form : $h(r) \simeq C_1 + C_2 r$. By using the holographic dictionary, we see that C_1 is associated with non-Abelian sources which is unphysical. So, we set $C_1 = 0$. This is the reason why when we minimize the action numerically, the only free parameters we minimize with respect to are r_c and C_2. When we inspect the IR asymptotics, $h = 0$ is an exact solution to the action and this is the one we consider since we have checked that the solution in the IR region ($r > r_c$) simply vanishes. Also, we must keep in mind that we treat the action in basically two independent parts. This is because of the discontinuity. Namely, the Lagrangian density is split into two pieces for $r < r_c$ and $r > r_c$ which are treated separately in absence of the delta function at r_c.

With this procedure we are able to compute the on-shell action directly, with which we calculate the Free energy that is defined through the following relation :

$$F = \left[\tilde{S}_h\right]_{on-shell} \tag{102}$$

Although, we do not have the expression for the Grand potential just yet. By integrating the final action we get the Free energy of the system. The Grand potential which is equal to minus the pressure, comes from Legendre transforming back (103). There results will be used to construct all the subsequent diagrams.

$$\Omega = \left[S_h\right]_{on-shell} \tag{103}$$

5.3 The $h(r)$ field potentials

In the numerical analysis we work in the in the probe limit, constructing the thermal gas background solutions [29], without including baryons and by setting the quark mass to zero. The potentials used in our analysis for the $h(r)$ field and the background fields are the following [3] :

$$\begin{aligned} V_g(\lambda) &= 12\Big(1 + V_1\lambda + \frac{V_2\lambda^2}{1+\lambda/\lambda_0} + V_{IR}e^{-\lambda_0/\lambda}(\lambda/\lambda_0)^{4/3}\sqrt{\log(1+\lambda/\lambda_0}\Big) \\ V_{f_0}(\lambda) &= W_0 + W_1\lambda + \frac{W_2\lambda^2}{1+\lambda/\lambda_0} + W_{IR}e^{-\lambda_0/\lambda}(\lambda/\lambda_0)^2 \\ \frac{1}{\kappa(\lambda)} &= \kappa_0\Big(1 + \kappa_1\lambda + \bar{\kappa}_0\big(1+\frac{\bar{\kappa}_1\lambda_0}{\lambda}\big)e^{-\lambda_0/\lambda}\frac{(\lambda/\lambda_0)^{4/3}}{\sqrt{\log(1+\lambda/\lambda_0)}}\Big) \end{aligned} \tag{104}$$

where the UV parameters are :

$$\begin{aligned} &V_1 = \frac{11}{27\pi^2}, \quad V_2 = \frac{4619}{46656\pi^4}, \\ &\kappa_0 = \frac{3}{2} - \frac{W_0}{8}, \quad W_1 = \frac{8+3W_0}{9\pi^2}, \quad W_2 = \frac{6488+999W_0}{15552\pi^4} \quad \text{and} \quad W_0 = 2.5 \end{aligned} \tag{105}$$

And for the glue sector potential the parameters are :

$$\lambda_0 = \frac{8\pi^2}{3} \quad \text{and} \quad V_{IR} = 2.05 \tag{106}$$

All these numbers were chosen to correspond data from lattice studies [32] and studies of the thermodynamics of pure Yang-Mills theory [35], [37]. In [37] the "potentials 7a" is constructed. the $w(\lambda)$ potential is chosen :

$$\frac{1}{w(\lambda)} = w_0\Big(1 + \bar{w}_0 e^{-\hat{\lambda}_0/\lambda}\frac{(\lambda/\hat{\lambda}_0)^{4/3}}{\log(1+\lambda/\hat{\lambda}_0)}\Big) \tag{107}$$

the UV parameters in this case are :

$$\begin{aligned} &\kappa_1 = \frac{11}{24\pi^2}, \quad W_0 = 2.5, \quad w_0 = 1.28, \quad M^3 = 1.32\frac{1+7/4}{45\pi^2 l^3}, \\ &\text{and} \quad l \quad \text{is the AdS radius,} \quad l = (1-2.5/12)^{-1/2} \end{aligned} \tag{108}$$

Finally, the IR parameters are the following :

$$\begin{aligned} &W_{IR} = 0.9, \quad \bar{\kappa}_0 = 1.8, \quad \bar{\kappa}_1 = -0.23, \\ &\hat{\lambda}_0 = 8\pi^2/1.18, \quad \bar{w}_0 = 1.8 \end{aligned} \tag{109}$$

5.4 Neutron Stars

Neutron stars are the densest and smallest stars that we have observed, not taking into account objects like black holes, quark stars, strange stars and white holes. They are the result of the collapse of a very massive star (order of 4 - 8 $M_\odot$). Using theoretical and observational data, the actual neutron star mass that is produced is at least 1.1 $M_\odot$ with an upper value of 2.16 $M_\odot$. Although, in the window between 1.1 to 1.39 $M_\odot$ the star in consideration is very likely to be a white dwarf as well. Although the work in [40] does not discuss the mass limits strictly, it provides a mass spectrum candidate as can also be seen in the figure (11). Apart from that, the radius is of the order of 10 kilometers. These information gives us a hint on what to expect from a neutron star created from our model, if V-QCD has any chance to be realistic after all.

Their formation is an interesting process. Let's consider the Hertzsprung–Russell diagram which is a plot of luminosity against the colour of the stars ranging from the high-temperature blue-white stars on the left side of the diagram to the low temperature red stars on the right side. Any star in that figure with mass > 8 $M_\odot$ is a possible candidate. During the end of the star life cycle, its gravitational collapse is being halted by neutron-degeneracy pressure combined with strong force repulsion. However, this is a dynamical and violent procedure which leads to a supernova explosion. If the remnant mass of the resulting core of this explosion is larger than 3 $M_\odot$ then it collapses further to a black hole. If not, then a neutron star is formed.

Holographic QCD is a very interesting way to connect with neutron star current research, as it provides a more fundamental theoretical model that describes the dynamics of the constituents of neutron stars. With a holographic model like this in hand, one is able to produce a neutron star Equation of State candidate and test the results with current data. Actually, one can go even further and create the merger of binary neutron stars and analyze the spectral properties of their gravitational waveforms [38]. This is very exciting especially in this time, when gravitational waves have been detected for the first time in 2015 and more and more people are working on it ever since. This means that theorists can collaborate with experimentalists to combine tools like the AdS/CFT correspondence with data from gravitational waves detectors and find the elusive equation of state for neutron stars.

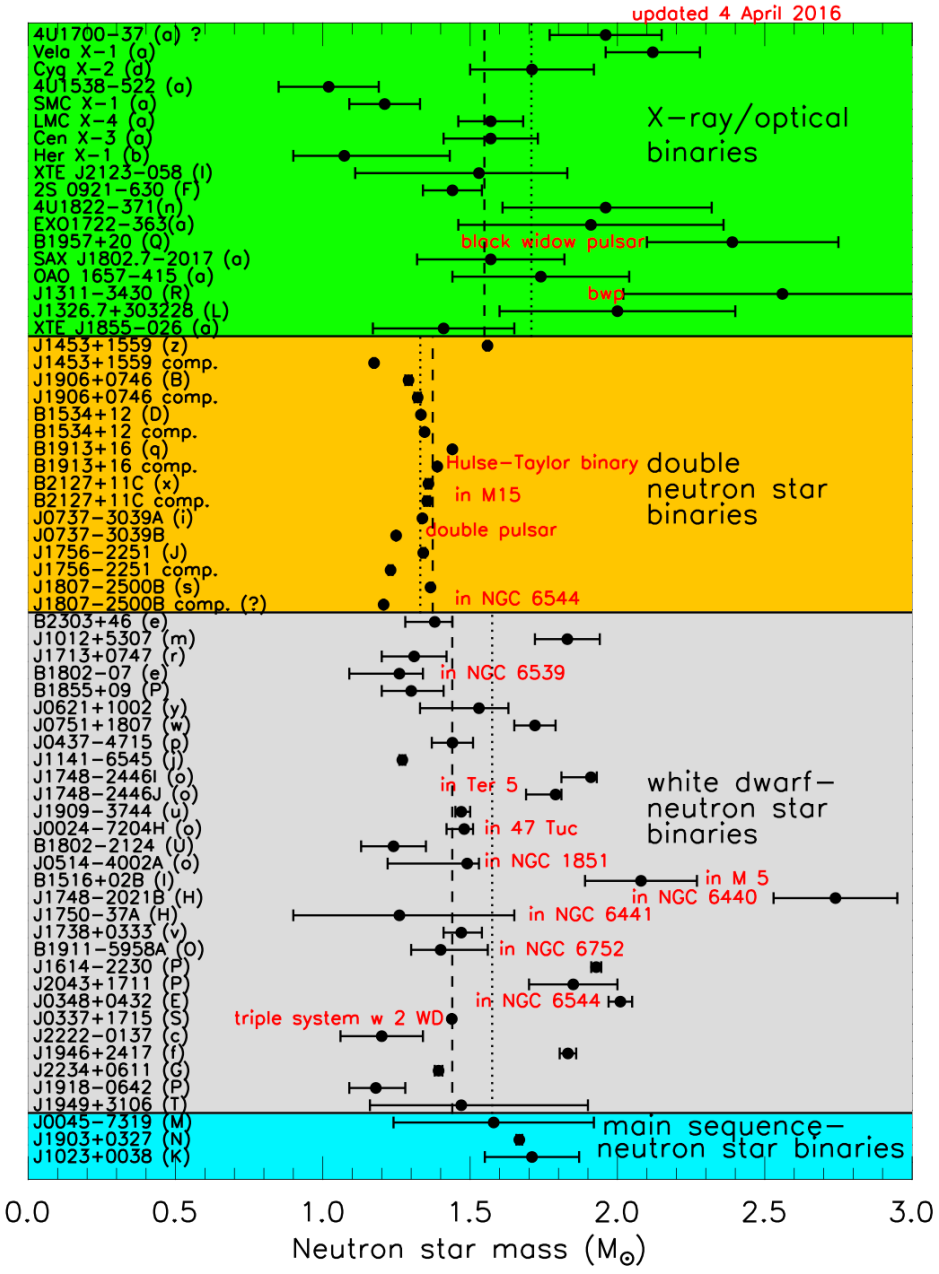

Figure 11: Taken from [40]. Measured and estimated masses of neutron stars.

6 Results and Conclusion

In this final chapter, we are going to present the results of our theory including the results for neutron stars. In more detail, we will present and use the Grand potential results for different values of the magnetic field and solve the Tomlan-Oppenheimer-Volkoff (TOV) equation. With this we will construct a Mass/Radius curve and check whether our model produces a realistic neutron star or not. We will also calculate more thermodynamic quantities and finally our thoughts will be summed up alongside ideas for future work.

6.1 Grand potential result

In figure (12) that follows we present the Grand potential with respect to chemical potential for different values of the magnetic field.

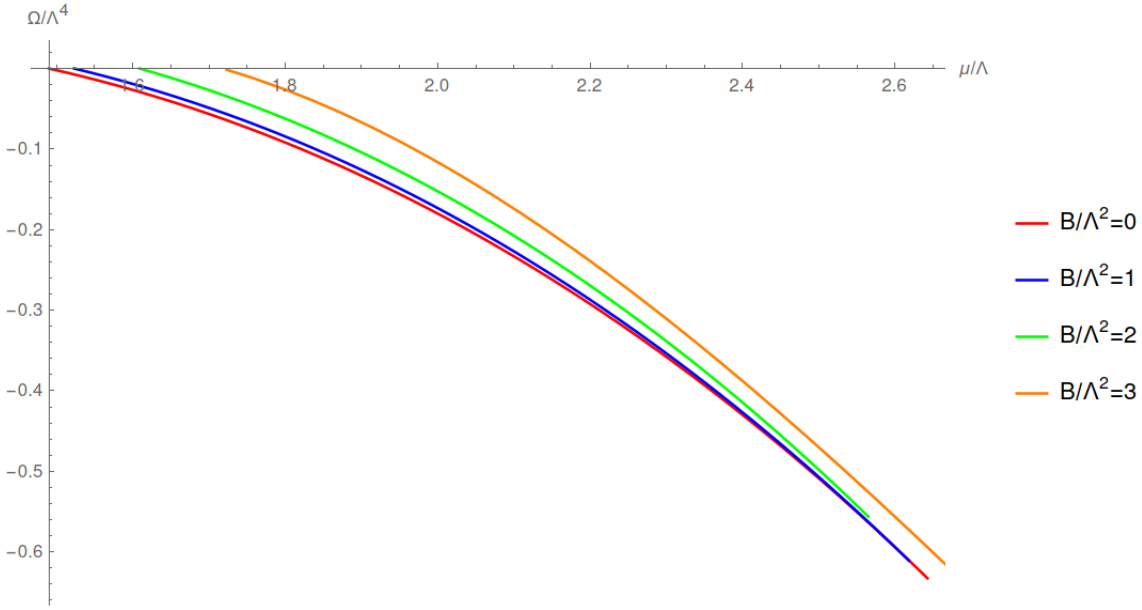

Figure 12: Grand Potential over chemical potential. The critical value of μ where our system shifts from the thermal gas to the baryonic phase increases with higher vaues of B.

We observe that the critical value of μ where our system shifts from the thermal gas phase to the baryonic, increases. This might indicate that baryons become more massive when a constant magnetic field is applied in the backgound. By using multiple data points from our numerical approach, we construct a phase diagram (13) of the critical values of μ with respect to the magnetic field. Again, it describes the shift from the thermal gas to the baryonic phase.

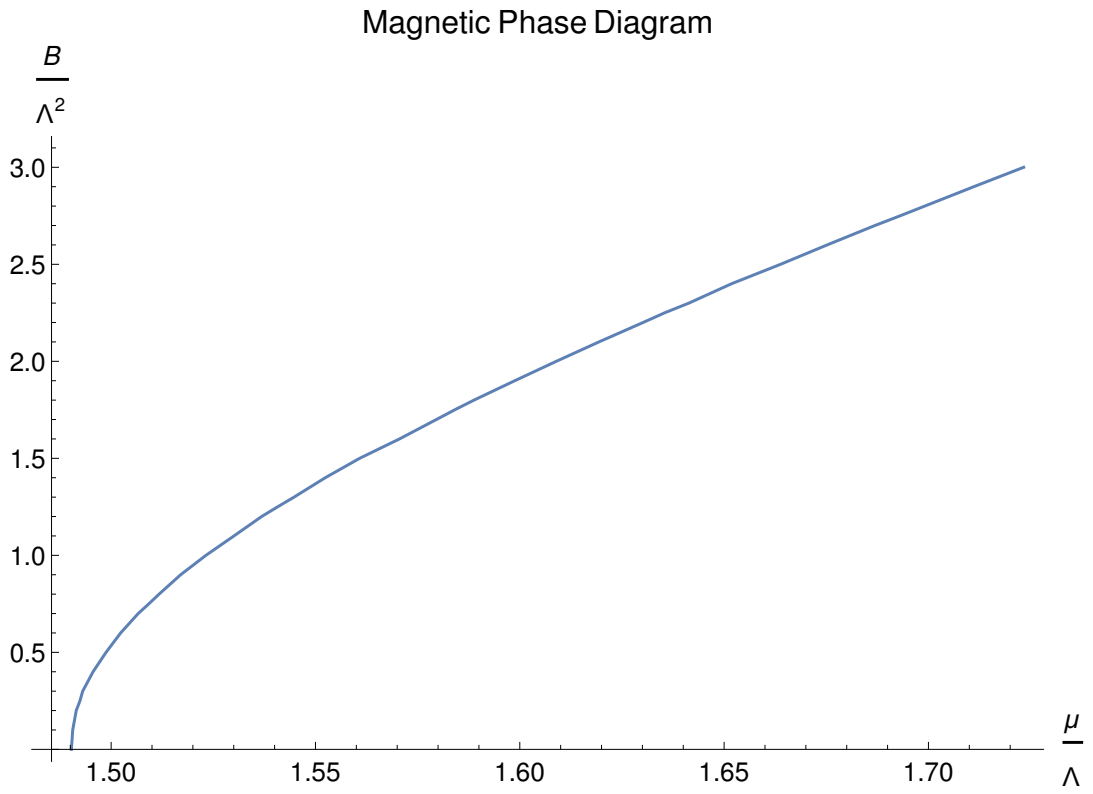

Figure 13: The curve depicts the critical values of μ, where the system goes through the phase transition.

6.2 Speed of sound

We also calculate the speed of sound in the direction of the magnetic field of our system [12]. We begin from the first law of thermodynamics written in the following form :

$$-dp = -sdT - nd\mu - MdB \tag{110}$$

where p is the pressure, s is the entropy density, T is the temperature, n is the number density, μ is the chemical potential, M is the magnetization and B is the magnetic field. Then we solve for the speed of sound by using the definition :

$$c_s^2 = dp/d\epsilon \tag{111}$$

where ϵ is the energy density. The formula we arrive in this manner and we use for our graph is :

$$c_s^2 = -\frac{\frac{\partial p}{\partial \mu}\mid_B}{\mu\frac{\partial^2 p}{\partial \mu^2}\mid_B + B\frac{\partial^2 p}{\partial \mu \partial B}} \tag{112}$$

For this calculation, we used the free energy we found in the previous section in order to calculate the terms $\frac{-\partial p}{\partial \mu}\mid_B$ and $\mu\frac{-\partial^2 p}{\partial \mu^2}\mid_B$ for different values of B. Although, because of the way our numerics work we were not able to calculate directly the derivative with respect to B of the free energy for the term $B\frac{-\partial^2 p}{\partial \mu \partial B}$. In order to overcome this obstacle we created a free energy function using B as free parameter, by creating multiple data points for different values of B and then fitting these point to the desired function. Hence, we were able to create the following figure that compares the speed of sound for different values of B.

We can see in figure (14), that by increasing the value of the background constant magnetic field the speed of sound drops. This leads us to conclude that the equation of state becomes stiff with respect to the application of the magnetic field.

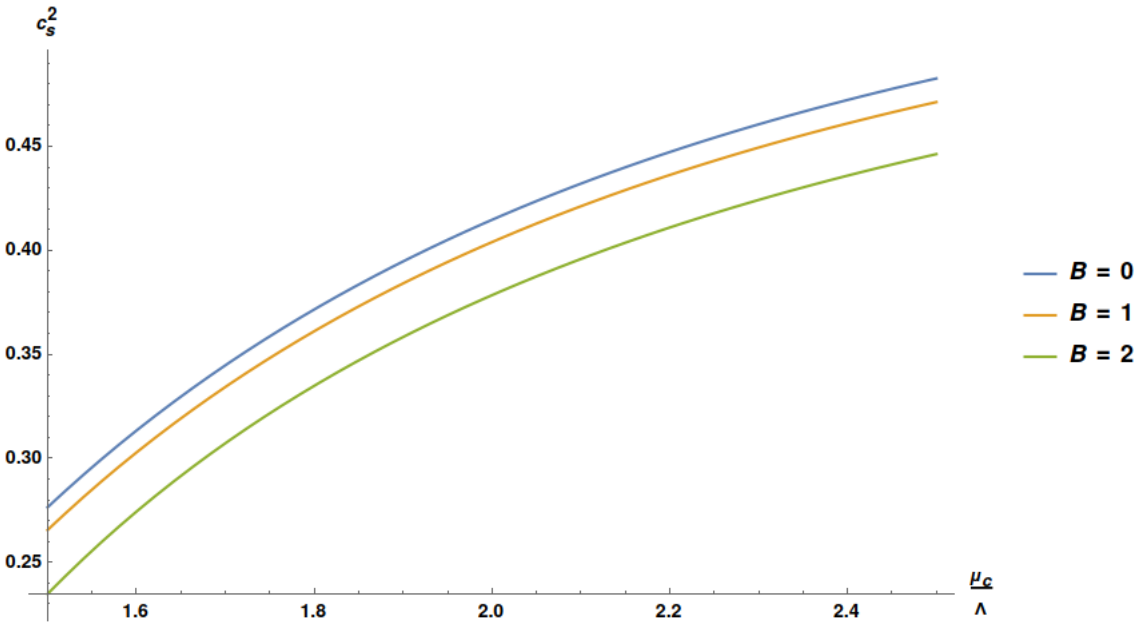

Figure 14: Speed of sound drops for larger values of the magnetic field.

6.3 Nuclear Saturation Density

We also calculate the nuclear saturation density (n_s) of our system which is simply defined as $\frac{dp}{d\mu}|_B$ evaluated at the transition from the thermal gas phase to the baryonic phase as a function of B. We use our numerical analysis to produce points from B=0 to B=3 with a 0.1 step. Apart from that we also use the 0.25, 0.75, 1.25, 1.75, 2.25, 2.75 extra points for better accuracy. The resulting figure is the following :

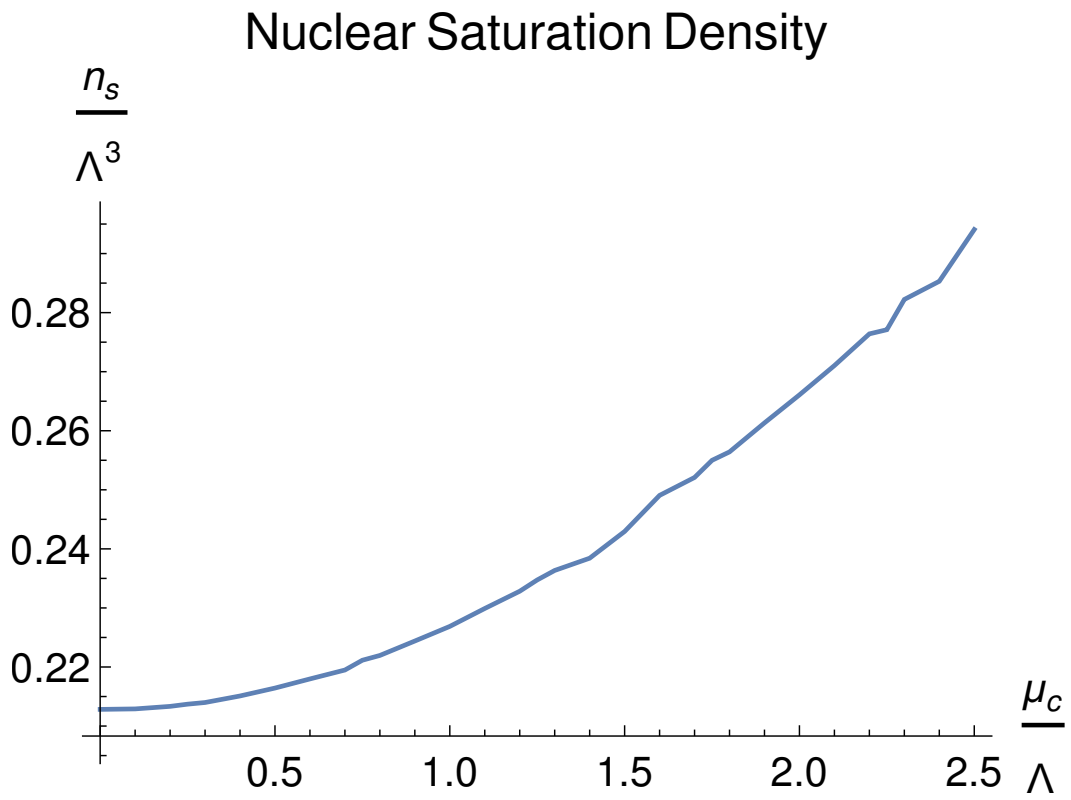

Figure 15: Nuclear Saturation Density increases with magnetic field.

From this diagram it is also obvious that by applying a constant magnetic field in the background the nuclear saturation density also increases. We stop at the value of B = 2.5 because for greater values than this our numerics break down. Although, the trend is pretty obvious.

6.4 Tomlan-Oppenheimer-Volkoff (TOV) equation and M/R curve

From General Relativity we know [36] that the TOV equation comes from considering a general static, spherically symmetric metric. We are then looking for non-vacuum solutions, which is achieved by considering the star interior as a perfect fluid in the energy-momentum tensor in the Einstein equations. Then, we arrive to an expression of the mass within a radius R, which is the integral of the energy density over the stellar interior. By taking into account the energy-momentum conservation we finally arrive to the TOV equation :

$$\frac{dp}{dr} = -\frac{(\epsilon + p)[Gm(r) + 4\pi G r^3 p]}{r[r - 2Gm(r)]} \tag{113}$$

We have also arrived to an Equation of State from V-QCD which is of the form :

$$\epsilon(p) = F(\mu) + \mu n + BM \tag{114}$$

where ϵ is the energy density, F is the free energy, μ is the chemical potential, n is the number density, B is the magnetic field and M is the magnetization. So, by combining these 2 equations we are able to get the M/R curve (16) for a holographic neutron star.

We can clearly see that while increasing the magnetic field, the neutron star becomes smaller. Taking into account also, that baryons appear to become more massive, we can assume that the neutron star becomes denser as well. We have to mention that a slight rescale of pressure had to be done in the end of our calculations in order to match the realistic values of neutron stars radii. Our initial radius for B = 0 was of the order of 18.5 km so + 7.5 km of the real value. The same rescaling was done for B = 1, B = 2 and B = 3. We do not consider this small rescale though as problematic as it amounts to refitting the normalization factors of the baryon action which is explained in [38]. This happens because our model is a bottom-up model as is already mentioned, which means that better and more accurate potentials can be chosen and give us more realistic results. In addition, radii go to zero at small mass because we don't have a realistic model for the neutron star crust. The crust is weakly coupled physics at lower density so holography is not directly useful for it, at least with the homogeneous approach. The results we have right now, we consider very encouraging. We also see that for B = 3 the curve is weird. This happens because our numerical method breaks down for values greater than 2.65 for B. We include the curve though just to show the trend.

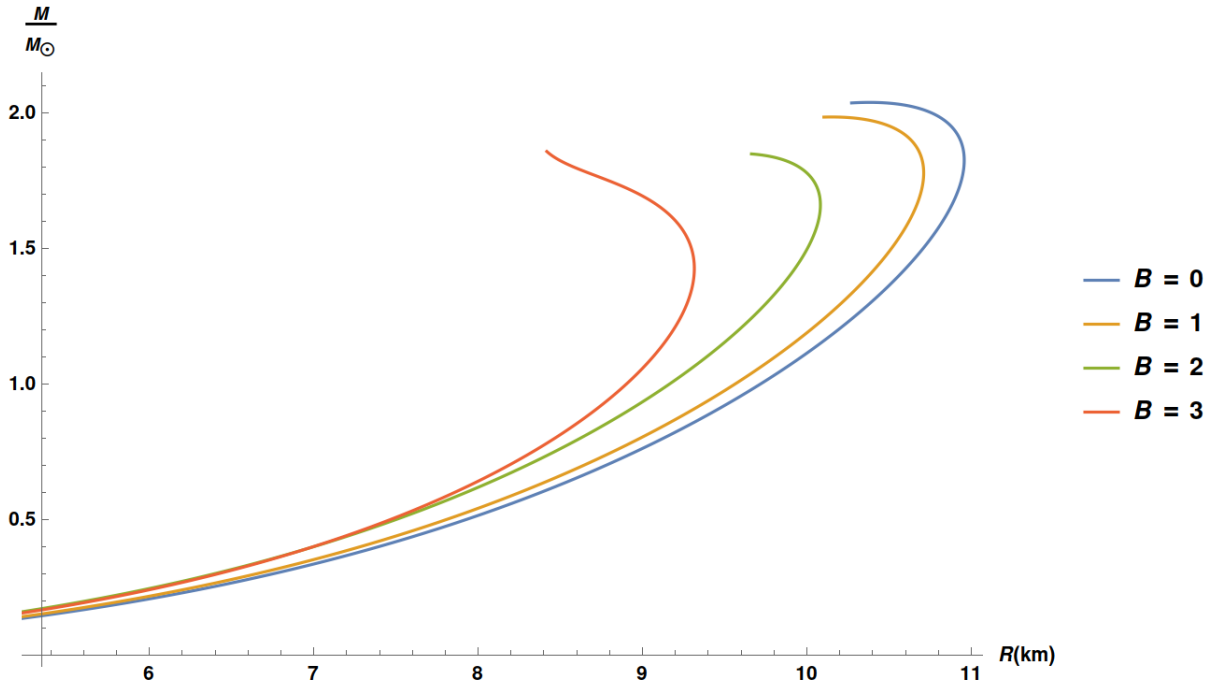

Figure 16: Mass/Radius curve for different values of the external magnetic field.

6.5 Conclusion

Summing up this thesis project, we considered nuclear matter in the presence of a constant background magnetic field in a holographic model using simple approximations (i.e. the homogeneous ansatz). We performed numerical analysis and we arrived to data for the free energy of the system. We then used this data to acquire an equation of state which we used to solve the TOV equations. Hence, we arrived to results for thermodynamic quantities and neutron stars. We found :

- Critical μ_c, on which the system goes from a thermal gas to a baryonic state increases with B.
- Speed of sound decreases with B.
- Nuclear saturation density increases with B.
- Neutron Stars appear to become denser and smaller with increasing B.

Our goal for future work is to continue our work on the more generalized and sophisticated ansatz (95). We believe that numerical analysis which will be done in the near future, will put us in the position to generalize our results or at least improve them.

7 Acknowledgments

I would like to thank Asoc. Prof. Umut Gürsoy for giving me the chance to work on such an interesting topic and for all his help throughout this project. Moreover, I am really grateful to have worked with a talented researcher like Dr. Matti Järvinen. He was always there to answer my questions, give me guidelines and spend a lot of time with me to make sure that I get the most out of this project. I would not have gotten this far without his guidance. Finally, I am really lucky to have worked with Govert Nijs who was like a supervisor "in the shadows" to me. He spent countless hours of fruitful discussion with me not only about the project, but also about my future. The numerical analysis would not have been made without his help. I hope I have the chance to work with these people again in the future.

Apart from the academic help that I received throughout my studies in Utrecht, I am really glad that my family were always there to support me in every way they could. Everything that I have achieved so far both in professional and personal level, I owe it to them. I also want to thank all my friends in Greece and Utrecht that always believed in me and supported me when things were tough.

A Forms in Chern-Simons terms

In section 4.5 we encountered the redefined $\tilde{\Omega}_5$ 5-form (80). In this equation there appeared two 4-forms $H_4^{(\Phi)}$, $H_4^{(B)}$ and one 2-form H_2. $H_4^{(\Phi)}$ was defined in the text but the rest were not explicitly stated because when evaluating the wedge product with f_B using our ansatz (85), they were zero. For completeness, we give their form here :

$$\begin{aligned}
e^{\tau^2} f_B \wedge H_4^{(B)} = \mathbb{T}r\Big(& -15if_B \wedge F^{(L)} \wedge F^{(L)} + 15if_B \wedge F^{(R)} \wedge F^{(R)} + 15\tau^2 f_B \wedge A_L \wedge A_L \wedge F^{(L)} \\
& - 15\tau^2 f_B \wedge A_L \wedge A_L \wedge F^{(R)} - 15\tau^2 f_B \wedge A_L \wedge A_R \wedge F^{(L)} + 15\tau^2 f_B \wedge A_L \wedge A_R \wedge F^{(R)} \\
& + 15\tau^2 f_B \wedge A_L^T \wedge A_R^T \wedge F^{(L)T} - 15\tau^2 f_B \wedge A_L^T \wedge A_R^T \wedge F^{(R)T} + 15\tau^2 f_B \wedge A_R \wedge A_R \wedge F^{(L)} \\
& - 15\tau^2 f_B \wedge A_R \wedge A_R \wedge F^{(R)} + 8if_B \wedge A_L \wedge A_L \wedge A_L \wedge A_L + 8i\tau^2 f_B \wedge A_L \wedge A_L \wedge A_L \wedge A_L \\
& - 8if_B \wedge A_R \wedge A_R \wedge A_R \wedge A_R - 8i\tau^2 f_B \wedge A_R \wedge A_R \wedge A_R \wedge A_R + 30i\tau f_B \wedge d\tau \wedge A_L \wedge F^{(L)} \\
& + 30i\tau f_B \wedge d\tau \wedge A_L \wedge F^{(R)} - 30i\tau f_B \wedge d\tau \wedge A_R \wedge F^{(L)} - 30i\tau f_B \wedge d\tau \wedge A_R \wedge F^{(R)} \\
& - 10\tau^3 f_B \wedge d\tau \wedge A_L \wedge A_L \wedge A_L + 30\tau^3 f_B \wedge d\tau \wedge A_L \wedge A_L \wedge A_R \\
& - 30\tau^3 f_B \wedge d\tau \wedge A_L \wedge A_R \wedge A_R + 10\tau^3 f_B \wedge d\tau \wedge A_R \wedge A_R \wedge A_R \Big)
\end{aligned} \tag{115}$$

which turns out to be the same as $H_4^{(\Phi)}$ but this time it is wedged with f_B which is why it is zero. H_2 is :

$$\begin{aligned}
e^{\tau^2} H_2 = \mathbb{T}r\Big(& -30iF^{(L)} + 30iF^{(R)} + 15A_L \wedge A_L - 15\tau^2 A_L \wedge A_L \\
& - 15A_R \wedge A_R + 15\tau^2 A_R \wedge A_R + 20i\tau^3 F^{(L)} - 20i\tau^3 F^{(R)} - 5\tau^3 A_L \wedge A_L \\
& + 5\tau^3 A_R \wedge A_R + 60iA_L - 20i\tau^3 A_L - 60i\tau A_R + 20i\tau^3 A_R \Big)
\end{aligned} \tag{116}$$

References

[1] M.E. Peskin, D.V. Schroeder, *"An Introduction to Quantum Field Theory"*, Addison-Wesley, Reading, 1995.

[2] David Tong, *David Tong: Lectures on Gauge Theory*, http://www.damtp.cam.ac.uk/user/tong/gaugetheory.html

[3] Takaaki Ishii, Matti Järvinen, Govert Nijs, *Cool baryon and quark matter in holographic QCD*, arXiv:1903.06169 [hep-ph].

[4] J. Maldacena, *"The Large N Limit of Superconformal Field Theories and Supergravity"*, Adv. Theor. Math. Phys. 2:231-252(1998), arXiv:hep- th/9711200v3.

[5] B. de Wit, E. Laenen and J. Smith, *"Field theory in Particle Physics"*, Utrecht University and University of Amsterdam - May 2018.

[6] Gert Aarts, *"Introductory lectures on lattice QCD at nonzero baryon number"*, arXiv:1512.05145 [hep-lat], DOI: 10.1088/1742-6596/706/2/022004.

[7] Makoto Natsuume, *"AdS/CFT Duality User Guide"*, arXiv:1409.3575 [hep-ph].

[8] E. Witten, *"Anti-de Sitter Space, Thermal Phase Transition, And Confinement in Gauge Theories"*, Adv. Theor. Math. Phys. 2: 505-532 (1998), arXiv:hep-th/9803131.

[9] K.G. Wilson, *"Confinement of quarks"*, Phys. Rev. D 10 (1974), 2445.

[10] G. 't Hooft, *"A Planar Diagram Theory for Strong Interaction"*, Nucl. Phys. B72, (1974), 461

[11] T. Alho, M.Järvinen, Kajantie, E. Kiritsis, C. Rosen, K. Tuominen, *"A holographic model for QCD in the Veneziano limit at finite temperature and density"*, arXiv:1312.5199 [hep-ph].

[12] Umut Gürsoy, Matti Järvinen and Govert Nijs, *"Holographic QCD in the Veneziano limit at finite Magnetic Field and Chemical Potential"*, arXiv:1707.00872 [hep-th].

[13] M. A. Stephanov, *"QCD phase diagram: an overview"*, arXiv:hep-lat/0701002.

[14] Roberto Casero, Elias Kiritsis, Ángel Paredes, *"Chiral symmetry breaking as open string tachyon condensation"*, arXiv:hep-th/0702155

[15] Alfonso V. Ramallo, *"Introduction to the AdS/CFT correspondence"*, arXiv:1310.4319 [hep-th]

[16] T. Alho, M. Jarvinen, K. Kajantie, E. Kiritsis, K. Tuominen, *"On finite-temperature holographic QCD in the Veneziano limit"*, arXiv:1210.4516 [hep-ph]

[17] Youngman Kim, Deokhyun Yi, *"Holography at work for nuclear and hadron physics"*, arXiv:1107.0155 [hep-ph], Adv.High Energy Phys.2011:259025,2011, DOI: 10.1155/2011/259025.

[18] K. Schalm, R. Davison, *"A simple introduction to AdS/CFT and its application to condensed matter physics."*, http://wwwhome.lorentz.leidenuniv.nl/ kschalm/teaching/CreteLectures.pdf

[19] Alex Pomarol, Andrea Wulzer, *"Baryon Physics in Holographic QCD"*, arXiv:0807.0316 [hep-ph], 10.1016/j.nuclphysb.2008.10.004.

[20] Alex Pomarol, Andrea Wulzer, *"Stable skyrmions from extra dimensions"*, JHEP 03 (2008) 051 [0712.3276].

[21] Edward Witten, *"Baryons And Branes In Anti de Sitter Space"*, arXiv:hep-th/9805112, DOI: 10.1088/1126-6708/1998/07/006.

[22] Matti Jarvinen, *"Recent progress in backreacted bottom-up holographic QCD"*, arXiv:1501.03693 [hep-ph].

[23] Hiroyuki Hata, Tadakatsu Sakai, Shigeki Sugimoto, Shinichiro Yamato, *"Baryons from instantons in holographic QCD"*, arXiv:hep-th/0701280, DOI: 10.1143/PTP.117.1157.

[24] U. Gursoy, E. Kiritsis, *"Exploring improved holographic theories for QCD: Part I"*, arXiv:0707.1324 [hep-th], DOI: 10.1088/1126-6708/2008/02/032.

[25] U. Gursoy, E. Kiritsis, F. Nitti, *"Exploring improved holographic theories for QCD: Part II"*, arXiv:0707.1349 [hep-th], DOI: 10.1088/1126-6708/2008/02/019.

[26] Krishna Rajagopal, *"Mapping the QCD Phase Diagram"*, arXiv:hep-ph/9908360, DOI: 10.1016/S0375-9474(99)85017-9.

[27] D. Sinclair, J. B. Kogut, *"Searching for the elusive critical endpoint at finite temperature and isospin density"*, PoS(LAT2006)147.

[28] Steven S. Gubser, *"Curvature Singularities: the Good, the Bad, and the Naked"*, arXiv:hep-th/0002160.

[29] Matti Jarvinen, Elias Kiritsis, *"Holographic Models for QCD in the Veneziano Limit"*, arXiv:1112.1261 [hep-ph], DOI: 10.1007/JHEP03(2012)002.

[30] Christine Davies, Peter Lepage, *"Lattice QCD meets experiment in hadron physics"*, arXiv:hep-ph/0311041.

[31] Umut Gursoy, *"Improved Holographic QCD and the Quark-gluon Plasma"*, arXiv:1612.00899 [hep-th], DOI: 10.5506/APhysPolB.47.2509.

[32] Marco Panero, *"Thermodynamics of the QCD Plasma and the Large-N Limit"*, Phys. Rev. Lett. 103 (2009) 232001 [0907.3719].

[33] Daniel Arean, Ioannis Iatrakis, Matti Jarvinen, Elias Kiritsis, *"The CP-odd sector and θ dynamics in holographic QCD"*, arXiv:1609.08922 [hep-ph], DOI: 10.1103/PhysRevD.96.026001.

[34] Ioannis Iatrakis, Elias Kiritsis, *"Vector-axial vector correlators in weak electric field and the holographic dynamics of the chiral condensate"*, arXiv:1109.1282 [hep-ph, DOI: 10.1007/JHEP02(2012)064

[35] T. Alho, M. Järvinen, K. Kajantie, E. Kiritsis and K. Tuominen, *"Quantum and stringy corrections to the equation of state of holographic QCD matter and the nature of the chiral transition"*, Phys. Rev. D91 (2015) 055017 [1501.06379].

[36] Sean M. Carroll, *"Spacetime and Geometry: An Introduction to General Relativity"*, Pearson (September 28, 2003)

[37] N. Jokela, M. Järvinen and J. Remes, *"Holographic QCD in the Veneziano limit and neutron stars"*,1809.07770.

[38] Christian Ecker, Matti Järvinen, Govert Nijs, Wilke van der Schee, *Gravitational Waves from Holographic Neutron Star Mergers*, arXiv:1908.03213 [astro-ph.HE]

[39] Frithjof Karsch, *"Lattice QCD at High Temperature and Density"*, arXiv:hep-lat/0106019.

[40] James M. Lattimer Madappa Prakash, *"The Ultimate Energy Density of Observable Cold Matter"*, arXiv:astro-ph/0411280, DOI: 10.1103/PhysRevLett.94.111101.